Scattering of Internal Waves with Frequency Change over Rough Topography

TOMOHIRO NAKAMURA

Pan-Okhotsk Research Center, Institute of Low Temperature Science, Hokkaido University, Sapporo, Japan

TOSHIYUKI AWAJI

Department of Geophysics, Graduate School of Science, Kyoto University, Kyoto, Japan

(Manuscript received 8 March 2007, in final form 3 November 2008)

ABSTRACT

The frequency change in internal gravity waves upon scattering from a rough topography is investigated analytically. For this, sets of appropriate and tractable governing equations for various parameter regimes are derived using the method of multiple scales under the assumption that the amplitude of the bottom topography is small. A solution is shown for a simple case in which an incident internal wave is approximately linear and monochromatic. The solution has the following features: the intrinsic frequencies of the scattered waves are given as the sum and difference of the incident-wave frequency and the Doppler shift (or lee-wave frequency). This Doppler shift causes the change in the frequency. Hence, the assumption of frequency conservation is not valid if the Doppler shift is significant, that is, when the horizontal scale of the bottom roughness (or the length scale in the plane of the slope) is on the order of or much less than that of the incident-wave flow excursion. This condition can be satisfied in a realistic parameter range.

The occurrence of such a frequency change has the following implications: first, it affects the estimate of the boundary mixing induced by the scattering because the energy redistribution in the vertical wavenumber space on scattering differs from that estimated using the assumption of frequency conservation. This effect happens because for a given horizontal wavenumber, the change in the frequency alters the vertical wavenumber of the scattered waves through the dispersion relation. Furthermore, if the incident waves are not monochromatic, even the leading-order scattered waves cannot be obtained by the superposition of the solutions for all the Fourier components of the incident waves because of the difference in the Doppler shift. Second, the effects of the background flow associated with the incident and primary reflected waves are significant when the frequency change occurs such that the background flow can create a critical level and/or advect scattered waves. The former causes mixing and background-flow acceleration, and the latter is favorable for the amplification of the scattered waves through superposition. Third, the resulting energy redistribution in frequency space could modify the spectrum shape of the oceanic internal waves, which is considered to affect both interior and boundary mixing.

1. Introduction

The reflection and scattering of oceanic internal gravity waves off bottom topography can redistribute internal wave energy to higher vertical wavenumbers, leading to enhanced mixing near the bottom boundary. Such internal wave-induced boundary mixing has been estimated to contribute significantly to the basinwide cross-isopycnal mixing (e.g., Eriksen 1985; Müller and Xu 1992). The total amount and the distribution of cross-isopycnal mixing strongly affect the global thermohaline circulation (e.g., Munk 1966; Bryan 1987; Munk and Wunsch 1998; Hasumi and Suginohara 1999); therefore, a better understanding of the reflection and scattering process is important not only for its theoretical interest but also for a better understanding and modeling of the thermohaline circulation.

Previous theories have revealed an interesting variety of reflected waves corresponding to various shapes of the bottom topography. Theories on the reflections over a plane slope showed that the wavenumber normal to the slope changes upon reflection based on the conservation of both the frequency and the wavenumber

Corresponding author address: Tomohiro Nakamura, Institute of Low Temperature Science, Hokkaido University, Sapporo 060-0819, Japan.
E-mail: nakamura@lowtem.hokudai.ac.jp

DOI: 10.1175/2008JPO3795.1

parallel to the slope. Such a change in the wavenumber results in intense mixing near a critical slope, where the bottom slope and the ray path of the reflected waves are parallel (e.g., Phillips 1977; Eriksen 1982, 1985).

Nonlinear effects, which become important in such a situation, were investigated further (e.g., Thorpe 1997). Theories on the reflections over a nonplanar but ''smooth'' topography in comparison with the wavelength of an incident plane wave have shown the occurrence of split reflection (Baines 1971b), different responses over convex and concave topographies (e.g., Gilbert and Garrett 1989), and the effects of finite topographic height and/or depth on the change in the vertical wavenumber (Müller and Liu 2000a,b). Numerical models were invoked to investigate the effects of three-dimensionality (Johnston and Merrifield 2003) and nonlinearity (Legg and Adcroft 2003) for this kind of topography.

When the bottom topography is rough compared to the wavelength of an incident wave (e.g., when a small sinusoidal variation with a wavenumber k_b is superimposed on a plane), Baines (1971a) found that the reflected waves comprise three components: a ''primary'' reflected wave and two types of ''scattered'' waves. The primary reflected wave is the same as that reflected from a plane. On the other hand, the scattered waves have different wavenumbers in the direction parallel to the plane. Their wavenumbers are determined as the sum and difference of the wavenumbers of the incident wave and the topographic wavenumbers (i.e., $k_i \pm k_b$, where k_i denotes the wavenumber of the incident wave). Mied and Dugan (1976) relaxed the condition of the small-amplitude bottom roughness in the case with no mean slope by expanding the scattered wave solution with respect to the slope of the bottom roughness. The horizontal wavenumber of the scattered waves is then given as the sum and difference of the wavenumbers of an incident wave and integer multiples of those of the topography (i.e., $k_i \pm nk_b$ for the nth order). Thorpe (2001) extended the theory to consider rough topographies with a mean slope, and Legg (2004) incorporated the Coriolis effect.

These theories were applied to the empirical spectral representations of the bottom topography and internal waves in order to estimate the redistribution of the incident-wave energy flux in wavenumber space (Rubenstein 1988; Müller and Xu 1992). In particular, Müller and Xu (1992) reformulated scattered wave solutions in a more revealing manner and estimated that scattering might be equally or more efficient than reflection in causing mixing near the bottom.

All of these previous theories have assumed that the frequency is conserved on reflection. In fact, absolute frequency (i.e., frequency in a reference frame fixed to the bottom) is conserved on reflection. Nevertheless, when a background flow is present, intrinsic frequency (frequency in a frame moving with the background flow) should be used; otherwise, the Doppler shift must be taken into account to determine the wave ray slope or wavenumbers of scattered waves. Previous theories on scattering neglected the effect of advection and hence implicitly assumed that intrinsic frequency is equal to absolute frequency and is hence conserved.

However, the validity of this assumption is questionable in a certain parameter range. For example, consider the generation of internal waves by a barotropic tidal flow over rough topography. The generated internal waves are expressed as the superposition of the higher harmonics (Bell 1975a; Balmforth et al. 2002; Khatiwala 2003), and their intrinsic frequencies are approximately given by the sum and difference of the tidal frequency and the Doppler shift (or lee-wave frequency) (Nakamura et al. 2000; Nakamura and Awaji 2001). In a similar manner, intrinsic frequency may be changed by scattering over rough topography.

St. Laurent and Garrett (2002) utilized without derivation Bell's (1975b) theory to estimate the energy flux scattered from the mode-1 internal tide at the Mid-Atlantic Ridge by using mode-1 internal tide currents in place of a sinusoidally oscillating barotropic current. Through the use of Bell's formula, the estimate should be affected by the effect of frequency change. Nevertheless, because their main focus was not on scattering, neither the validation of the use of Bell's formula for that case nor the condition, mechanism, or effects of frequency change was investigated.

In this paper, we shall analytically demonstrate that the frequency conservation for internal wave reflection is violated in certain parameter regimes. The condition and effects of the violation of the frequency conservation are then investigated.

After a heuristic derivation of governing equations, a scattered wave solution with advection effect is presented in section 2 for a simple case in which both the incident wave and the bottom topography are monochromatic and in which the Boussinesq approximation is used with a uniform buoyancy frequency. The occurrence of frequency change and its relation to higher harmonics are shown in section 3. The condition for frequency change and its extent in various parameter ranges are investigated in section 4. A more rigorous derivation of the leading-order equations is given in section 5, which validates the governing equations used in section 2 and further reveals that the appropriate governing equations differ for various parameter regimes (or equivalently, shows which terms are negligible

to what order). Possible effects and implications are then discussed in section 6. Finally, the results are summarized in section 7.

2. Scattered wave solution with advection by primary waves

a. Governing equations

Consider internal wave reflection over small-amplitude, rough topography. Then the primary wave field consists of the incident wave and its reflection on a plane horizontal boundary (i.e., the primary reflected wave). For a sinusoidal incident wave, these waves form an exact solution of the nonlinear governing equations with Boussinesq approximation for uniform stratification. The equations for the scattered waves are then obtained by linearizing about this solution. The result will be the usual linearized internal wave equations, with extra advection terms such as $\mathbf{u}_{i+r} \cdot \nabla\phi_s + \mathbf{u}_s \cdot \nabla\phi_{i+r}$, where the subscripts $i + r$ and s denote the sum of the incident and primary reflected waves and scattered waves, respectively, and ϕ denotes momentum or density. In the usual linear theory such advection terms are neglected, and the scattered wave field satisfies the usual homogeneous linear equations forced by the bottom boundary condition.

We consider here the effect of the advection by the primary wave field, $\mathbf{u}_{i+r} \cdot \nabla\phi_s$. This is done by assuming momentarily that it is possible to neglect the spatial derivative of the primary wave field in the scattered wave equations when the primary wave field is slowly varying relative to the topography and hence to the scattered wave field.

Then the two-dimensional equations for the scattered waves in an inviscid, rotating, and uniformly stratified Boussinesq fluid become

$$\begin{aligned} \frac{Du_s}{Dt} - fv_s &= -\frac{1}{\rho_0}\frac{\partial p_s}{\partial x_s} \\ \frac{Dv_s}{Dt} + fu_s &= 0, \\ \frac{Dw_s}{Dt} &= -\frac{\partial p_s}{\partial z_s} - \rho_s', \\ \frac{D\rho_s'}{Dt} &= -\frac{\partial \overline{\rho}}{\partial z_s} w_s. \\ \frac{\partial u_s}{\partial x_s} + \frac{\partial w_s}{\partial z_s} &= 0, \end{aligned} \tag{2.1}$$

where

$$\frac{D}{Dt} = \frac{\partial}{\partial t} + u_l \frac{\partial}{\partial x_s} + w_l \frac{\partial}{\partial z_s}. \tag{2.2}$$

The corresponding bottom boundary condition is

$$w_s(z = 0) = u_l \frac{\partial h}{\partial x_s}. \tag{2.3}$$

Here, the standard notations are used. The subscripts l and s denote large- and small-scale variables associated with the primary and scattered wave fields, respectively. The density is separated into the reference value, background stratification, and perturbation as

$$\rho_{total} = \rho_0 + \overline{\rho}(z) + \rho'(\boldsymbol{x}, t). \tag{2.4}$$

The validity of the neglect of the nonlinear terms like $\mathbf{u}_s \cdot \nabla\phi_{i+r}$ will be examined later in section 5. Here we note beforehand that the above governing equations are valid in a parameter regime where $k_sU_l/\omega_l\ (= k_sU_{i+r}/\omega_i) \sim 1$, $\omega_s \sim \omega_l$, and $k_lU_l/\omega_l \ll 1$ (k, ω, and U are the horizontal wavenumber, intrinsic frequency, and the amplitude of horizontal velocity, respectively). Because of the last condition, $k_lU_l/\omega_l \ll 1$, the primary waves can be approximated to be linear in the leading order, even when the advection by the primary waves is taken into consideration. In other parameter regimes, the appropriate governing equations take somewhat different forms. This is especially so in the regime where the incident wave is nonlinear in the leading order.

The above governing equations can be solved using the Fourier transform, as shown in the rest of this section, because the spatial derivative of the large-scale wave field (i.e., the primary wave field) is assumed to be negligible.

b. General solution

Governing equations (2.1) can be reduced to a single equation for w_s as

$$\frac{D^2}{Dt^2}(\nabla_s^2 w_s) + N^2 \frac{\partial^2 w_s}{\partial x_s^2} + f^2 \frac{\partial^2 w_s}{\partial z_s^2} = 0 \tag{2.5}$$

because the large-scale wave field does not depend on the small-scale coordinates (x_s,z_s) and thus D/Dt and $\nabla_s = (\partial/\partial x_s, \partial/\partial z_s)$ commute.

For the same reason, (2.5) can be solved using the Fourier transform, and thus w_s may be written as the sum of Fourier components:

$$w_s = A_s(\mathbf{x}_l) \int\int \hat{w}_s(\mathbf{k}_s, t)\, e^{i\mathbf{k}_s \cdot \mathbf{x}_s} dk_s dm_s, \tag{2.6}$$

where $\mathbf{k}_s = (k_s,m_s)$. The equation for each component is then given as

$$\left(\frac{\partial}{\partial t} + ik_s u_l + im_s w_l\right)^2 \hat{w}_s(\mathbf{k}_s, t) + \Omega^2(\mathbf{k}_s)\hat{w}_s(\mathbf{k}_s, t) = 0, \tag{2.7}$$

where

$$\Omega(\mathbf{k}) = \left(\frac{N^2k^2 + f^2m^2}{k^2 + m^2}\right)^{1/2}. \tag{2.8}$$

To solve (2.7), we introduce a frame $[\mathbf{X}_s = (X_s,Z_s)]$ moving with $\mathbf{u}_l$; that is,

$$\mathbf{X}_s = \mathbf{x}_s - \int_0^t \mathbf{u}_l[\mathbf{x}_l(t'), t']dt', \tag{2.9}$$

which is an extension of the moving frame introduced by Bell (1975a). In the moving frame $\mathbf{X}_s$, $\hat{w}_s$ is described as

$$\hat{w}_s^m(\mathbf{k}_s, t) = \hat{w}_s(\mathbf{k}_s, t)\exp\left\{i\mathbf{k}_s \cdot \int_0^t \mathbf{u}_l[\mathbf{x}_l(t'), t']dt'\right\} \tag{2.10}$$

and (2.7) becomes

$$\frac{\partial^2\hat{w}_s^m}{\partial t^2} + \Omega^2(\mathbf{k}_s)\hat{w}_s^m = 0. \tag{2.11}$$

This can be solved using a Fourier transform with respect to time,

$$\hat{w}_s^m = \int_{-\infty}^{\infty} F(\omega)\, e^{-i\omega t}d\omega, \tag{2.12}$$

yielding the dispersion relation

$$\omega^2 = \Omega^2(\mathbf{k}_s). \tag{2.13}$$

Because ω and k_s are specified from the bottom boundary condition described below, m_s is determined to satisfy the dispersion relation along with the radiation condition.

c. Topography and large-scale waves

To determine the properties of scattered waves from the bottom boundary condition, we next specify the bottom topography and large-scale waves in a very simple fashion to provide basic insight into more complicated situations.

We consider bottom topography and an incident wave that are both monochromatic as

$$h = H\cos(k_b x_s) = \frac{1}{2}H(e^{ik_b x_s} + e^{-ik_b x_s}), \quad (k_b > 0), \tag{2.14}$$

$$\begin{aligned}\mathbf{u}_i &= \mathbf{U}_i(\mathbf{k}_i)\cos(k_i x_l + m_i z_l - \omega_i t)\\ &= \frac{1}{2}[\mathbf{U}_i(\mathbf{k}_i)e^{i(k_i x_l + m_i z_l - \omega_i t)} + \mathbf{U}_i(-\mathbf{k}_i)e^{-i(k_i x_l + m_i z_l - \omega_i t)}].\end{aligned} \tag{2.15}$$

Here, subscripts i and b denote the incident wave and the bottom topography, respectively. The incident wave satisfies the linear internal-wave Eqs. (5.34) in section 5c.

For convenience, we define a notation θ, which works in a manner similar to Einstein's summation rule but represents a summation for the cases of $\theta = 1$ and $\theta = -1$, such that

$$\begin{aligned}e^{i\theta kx} &= e^{ikx} + e^{-ikx},\\ \frac{\partial}{\partial x}e^{i\theta kx} &= i\theta k e^{i\theta kx} = ike^{ikx} + i(-k)e^{-ikx}.\end{aligned}$$

The wavenumbers or frequencies with the θ notation are defined as positive or zero. When there are θ notations with different subscripts, each notation is independently summed such that

$$\begin{aligned}e^{i(\theta_k kx - \theta_\omega \omega t)} &= e^{i(kx - \theta_\omega \omega t)} + e^{i(-kx - \theta_\omega \omega t)}\\ &= e^{i(kx-\omega t)} + e^{i(kx+\omega t)} + e^{i(-kx-\omega t)} + e^{i(-kx+\omega t)}\\ &= 4\cos(kx)\cos(\omega t).\end{aligned}$$

The use of this notation allows us to write the relation between the sign of the wavenumber and the frequency explicitly and neatly.

Using this θ notation, the above topography and incident wave are written as

$$h = \frac{1}{2}He^{i\theta_b k_b x_s}, \tag{2.16}$$

$$\mathbf{u}_i = \frac{1}{2}\mathbf{U}_i(\theta_i\mathbf{k}_i)e^{i\theta_i(k_i x_l + m_i z_l - \omega_i t)}. \tag{2.17}$$

Here, $\mathbf{U}_i = (U_i,V_i,W_i)$ comprises amplitudes of the velocity components, which can be written in terms of U_i (which is set to a constant value) from the polarization relation as

$$V_i = \frac{f}{i\theta_i\omega_i}U_i, \quad W_i = -\frac{k_i}{m_i}U_i, \tag{2.18}$$

and ω_i is the incident-wave frequency given from the dispersion relation as

$$\omega_i = \Omega(\mathbf{k}_i). \tag{2.19}$$

The primary reflected wave, whose governing equations are the same as those of the incident wave, is determined from the bottom boundary condition, $w_l = 0$ at $z = 0$, and from the radiation condition as

$$\mathbf{u}_r = \frac{1}{2}\mathbf{U}_i(\theta_i\mathbf{k}_i)e^{i\theta_i(k_i x_l - m_i z_l - \omega_i t)}, \tag{2.20}$$

where subscript r denotes the primary reflected wave. The horizontal velocity (along the x direction) of these large-scale waves at $z = 0$ is thus given by

$$u_l = u_i + u_r = U_i e^{i\theta_i(k_i x_l - \omega_i t)} [= 2U_i \cos(k_i x_l - \omega_i t)]. \tag{2.21}$$

d. Bottom boundary condition and the solution

Given the bottom topography and the large-scale wave field, a specific solution is determined from the bottom boundary condition.

The substitution of (2.6), (2.16), and (2.21) into the bottom boundary condition (2.3) yields

$$A_s(x_l, 0) \int\int \hat{w}_s(\mathbf{k}_s, t) e^{ik_s x_s} dk_s dm_s = U_i e^{i\theta_i(k_i x_l - \omega_i t)} \frac{1}{2} i\theta_b k_b H e^{i\theta_b k_b x_s}. \tag{2.22}$$

The bottom boundary condition is then described in the moving frame for consistency with the general solution as

$$A_s(x_l, 0) \int\int \hat{w}_s^m(\mathbf{k}_s, t) e^{ik_s X_s} dk_s dm_s, = \frac{1}{2} i\theta_b k_b H U_i e^{i\theta_i(k_i x_l - \omega_i t)} e^{i\theta_b k_b X_s + i\theta_b k_b \int_0^t u_l|_{z=0} dt'}, \tag{2.23}$$

which implies

$$A_s(x_l, 0) = \frac{1}{2} i\theta_b k_b H U_i e^{i\theta_i k_i x_l}, \tag{2.24}$$

$$\hat{w}_s^m(\mathbf{k}_s, t) = \delta(k_s - \theta_b k_b) e^{-i\theta_i \omega_i t + i\theta_b k_b \int_0^t u_l|_{z=0} dt'}. \tag{2.25}$$

Applying this bottom boundary condition to (2.12) and applying the inverse Fourier transform yields

$$F(\omega) = \frac{1}{2\pi} \int_{-\infty}^{\infty} e^{i\phi} dt, \tag{2.26}$$

$$\phi = -\theta_i \omega_i t + \theta_b k_b \int_0^t u_l|_{z=0} dt' + \omega t. \tag{2.27}$$

The solution in the fixed frame is thus obtained as

$$\begin{aligned} w_s &= A_s \int\int \hat{w}_s e^{i\mathbf{k}_s \cdot \mathbf{x}_s} dk_s dm_s \\ &= A_s \int\int \hat{w}_s^m e^{-i\mathbf{k}_s \cdot \int_0^t \mathbf{u}_l[x_l(t'), t'] dt'} e^{i\mathbf{k}_s \cdot \mathbf{x}_s} dk_s dm_s \\ &= \frac{1}{2} i\theta_b k_b H U_i e^{i\theta_i k_i x_l} \\ &\quad \times e^{-i(\theta_b k_b \int_0^t u_l(x_l(t'), t') dt' - sign(\omega) m_s \int_0^t w_l(\mathbf{x}_l(t'), t') dt'} \\ &\quad \times \int_{-\infty}^{\infty} F(\omega) e^{i[\theta_b k_b x_s - sign(\omega) m_s z_s - \omega t]} d\omega, \end{aligned} \tag{2.28}$$

where the vertical wavenumber m_s, whose absolute value is determined from the dispersion relation, is defined as positive in order to explicitly represent the radiation condition.[1]

In the moving frame, the solution takes a more revealing form:

$$w_s^m = \frac{1}{2} i\theta_b k_b H U_i e^{i\theta_i k_i x_l} \times \int_{-\infty}^{\infty} F(\omega) e^{i[\theta_b k_b X_s - sign(\omega) m_s Z_s - \omega t]} d\omega. \tag{2.29}$$

3. Change in intrinsic frequency

a. Frequency of scattered waves

The frequency of major components of the scattered waves is determined from the function $F(\omega)$, which sets the complex amplitude of the scattered waves and is specified in (2.26). According to the stationary phase method (e.g., Lighthill 1978), the major contributions to the integral (2.26) comes from the intrinsic frequency ω that satisfies

$$\frac{\partial \phi}{\partial t} = \theta_b k_b u_l|_{z=0} - \theta_i \omega_i + \omega = 0. \tag{3.1}$$

The above condition is satisfied twice during one cycle of the incident wave for one value of intrinsic frequency (or once for $u_l|_{z=0} = \pm 2U_i$), and the integral is estimated by the sum of these main contributions.

Conversely, this means that the main components of scattered waves generated at a time t_0 have the intrinsic frequency of

$$\omega = \pm(-k_b u_l|_{z=0,\, t=t_0} \pm \omega_i), \tag{3.2}$$

where $u_l|_{z=0}$ is given by (2.21).[2] After the generation, the scattered waves with the above intrinsic frequency propagate through the primary wave field, and w_s^m is

[1] It should be noted that the wavenumber in the fixed frame is, strictly speaking, different from that in the frame moving with the background flow that has nonzero convergence/divergence in the x or z direction. The extent of the difference depends on the ratio of wavenumbers of incident and scattered waves (i.e., $\delta_k = k_i/k_s$ and $\delta_m = m_i/m_s$ in the x and z directions, respectively, as discussed in section 5). The order of the associated error is the same as that arising from the neglect of the spatial variation of an incident wave in the derivation of the leading-order equations for the scattered waves and is small when δ_k and $\delta_m \ll 1$.

[2] Equation (3.2) is obtained because the exponential function in the integral in (2.29) becomes, after the substitution of (3.1) into (2.29),

$$\begin{aligned} &e^{i[\theta_b k_b X_s - sign(\omega) m_s Z_s - (-\theta_b k_b u_l|_{z=0} + \theta_i \omega_i)t]} \\ &= e^{i[k_b X_s - sign(\omega) m_s Z_s - (-k_b u_l|_{z=0} + \omega_i)t]} \\ &= e^{i[k_b X_s - sign(\omega) m_s Z_s - (-k_b u_l|_{z=0} - \omega_i)t]} \\ &= e^{i[-k_b X_s - sign(\omega) m_s Z_s - (k_b u_l|_{z=0} + \omega_i)t]} \\ &= e^{i[-k_b X_s - sign(\omega) m_s Z_s - (k_b u_l|_{z=0} - \omega_i)t]}. \end{aligned}$$

obtained by the sum of these main components generated during the time duration under consideration.

Equation (3.2) indicates that the intrinsic frequency of the scattered waves is given as the sum or the difference of the incident-wave frequency and the Doppler-shift frequency (i.e., lee-wave frequency); that is,

$$\begin{aligned}(\text{intrinsic freq.}) = &\ (\text{Doppler shift})\\ &\pm (\text{incident wave freq.}).\end{aligned}$$

The mechanism of frequency change is essentially the same as that in the case of internal wave generation by a tidal flow (Nakamura et al. 2000). In fact, the bottom boundary condition is almost identical to the case considered in Bell (1975a) and Nakamura et al. (2000).

b. Relation to the higher harmonics

It should be noted that the above expression yields the same wave field described using the higher harmonics like Bell's (1975a) solution within the approximation of the stationary phase method.

To bring out this point, let us focus on the advection effect in the kinematic bottom boundary condition, assuming that the total time derivative is approximated as

$$\frac{D}{Dt} \approx \frac{\partial}{\partial t} + u_{i+r}(t)\frac{\partial}{\partial x} \quad \text{at } z = 0 \tag{3.3}$$

and the kinematic boundary condition is

$$w_s = u_{i+r}(t)\frac{\partial h}{\partial x} \quad \text{at } z = 0. \tag{3.4}$$

These correspond to (2.2) and (2.3), respectively, but x_s is here written as x and the spatial variation of u_{i+r} is ignored for simplicity. Despite this simplification, the results are essentially the same both because $\mathbf{k}_l$ affects only the slowly varying amplitude of scattered waves in this parameter range as shown in (2.29) and because of the boundary condition $w_l = 0$ at $z = 0$.

The essence of the frequency change may be summarized as follows: Consider a monochromatic, plane incident wave that yields

$$u_{i+r}(z = 0) = U_{i+r}\cos\omega_i t. \tag{3.5}$$

Introduce the Fourier transform

$$\hat{()} = \int_{-\infty}^{\infty} ()e^{-ikx}dx \tag{3.6}$$

and the transformation to a reference frame moving with the background flow

$$\hat{()}^m = \hat{()}\exp\left[ik\int_0^t u_{i+r}(z = 0, \tau)d\tau\right]. \tag{3.7}$$

Then the bottom boundary condition becomes

$$\hat{w}_s^m(z = 0) = iku_{i+r}(z = 0, t)\hat{h}\exp\left[ik\int_0^t u_{i+r}(z = 0, \tau)d\tau\right]. \tag{3.8}$$

The Fourier transform of $\hat{w}^m(z = 0)$ with respect to time yields

$$\hat{w}_s^m(z = 0) = \int_{-\infty}^{\infty} F(z = 0, \omega)e^{-i\omega t}d\omega, \tag{3.9}$$

with inverse

$$\begin{aligned}F(z = 0, \omega) &= \frac{1}{2\pi}\int_{-\infty}^{\infty}\hat{w}_s^m(z = 0)e^{i\omega t}dt\\ &= \frac{ik\hat{h}}{2\pi}\frac{U_{i+r}}{4}\int_{-\infty}^{\infty}\exp i\left[\pm\omega_i t + k\int_0^t u_{i+r}(z = 0, \tau)d\tau + \omega t\right]dt.\end{aligned} \tag{3.10}$$

According to the stationary phase method, the main contributions to the integral on the right-hand side comes from the intrinsic frequency ω that satisfies

$$\begin{aligned}0 &= \frac{\partial}{\partial t}\left[\pm\omega_i t + k\int_0^t u_{i+r}(z = 0, \tau)d\tau + \omega t\right],\\ &= \pm\omega_i + ku_{i+r}(z = 0, t) + \omega,\end{aligned} \tag{3.11}$$

and thus the main component of internal waves generated at a time t_0 has the intrinsic frequency of

$$\omega = -ku_{i+r}(z = 0, t = t_0) \pm \omega_i, \tag{3.12}$$

as shown in the previous section.

On the other hand, Bell's solution method directly expresses the integral on the right-hand side of (3.9) using a series expansion as

$$\begin{aligned}\hat{w}^m(z = 0) &= \int_{-\infty}^{\infty} F(z = 0, \omega)e^{-i\omega t}d\omega\\ &= iku_{i+r}(z = 0, t)\hat{h}\exp\left[ik\int_0^t u_{i+r}(z = 0, \tau)d\tau\right],\end{aligned} \tag{3.13}$$

$$= \hat{h}\frac{\partial}{\partial t}\exp\left[ik\int_0^t u_{i+r}(z = 0, \tau)d\tau\right], \tag{3.14}$$

$$= \hat{h}\frac{\partial}{\partial t}\sum_{n=-\infty}^{\infty} e^{in\omega_i t}J_n\left(\frac{kU_{i+r}}{\omega_i}\right), \tag{3.15}$$

so that the total wave field is given by the sum of higher harmonics.

The main difference between Bell's method and the stationary phase method is the way of estimating the integral in (3.13) [and (3.9)]. A minor difference is the

transformation from (3.13) to (3.14), which is absent in the stationary phase method and can be omitted in Bell's solution method.

Thus, within the approximation of the stationary phase method, internal wave components generated at time t have intrinsic frequencies of $-ku_{i+r}(z = 0, t) \pm \omega_i$, whereas the total scattered-wave field, which is composed of the superposition of such wave components and is subjected to the advection by the background flow, is described with the sum of the higher harmonics. The relation between the above results of the stationary phase method and Bell's solution may be analogous, although it is not quite precise, to the relation between a narrow internal-wave beam described by integration along wave rays and that expressed as the sum of multiple vertical modes. [Although the approximation used in the stationary phase method could have a significant error in the vicinity of $kU_{i+r} = \omega_i$, the results of our numerical experiments (in preparation) suggest that the prediction of the stationary phase method is robust in a qualitative sense even in the case $kU_{i+r} = \omega_i$.]

Note also that the higher harmonics in Bell's solution contain not only the effect of the change in intrinsic frequency but also the effect of the oscillation of the advecting flow. To reveal this fact, consider the situation in which an internal wave of the tidal frequency ω_0 is being advected by a barotropic tidal flow $U(t) = U_0\cos(\omega_0 t)$. The vertical flow associated with the internal wave at a certain point in the moving frame may be written as

$$w^m = -\frac{k}{m} U_i \cos(\omega_0 t), \tag{3.16}$$

where U_i is the complex amplitude of the horizontal flow of the internal wave with k and m the horizontal and vertical wavenumbers, respectively. The vertical flow can be rewritten as

$$w^m = \frac{i}{m}\frac{U_i}{U_0} ikU_0 \cos(\omega_0 t) \tag{3.17}$$

and thus is described in the frame fixed to the bottom as

$$\begin{aligned} w &= w^m e^{-ik\int_0^t U(\tau)d\tau} \\ &= -\frac{i}{m}\frac{U_i}{U_0}\frac{\partial}{\partial t} e^{-ik\int_0^t U(\tau)d\tau} \end{aligned} \tag{3.18}$$

$$= -\frac{i}{m}\frac{U_i}{U_0}\sum_{n=-\infty}^{\infty} in\omega_0 e^{in\omega_0 t} J_n\left(\frac{kU_0}{\omega_0}\right). \tag{3.19}$$

This shows that an internal wave that is advected by a sinusoidal tidal flow and has intrinsic frequency of the tidal frequency is expressed as the sum of the higher harmonics in the fixed frame. Similarly, an internal wave with the tidal frequency in the fixed frame becomes the sum of the higher harmonics in the frame moving with the sinusoidal tidal flow.

In this sense, the physics of frequency change is masked in the expansion into a series of higher harmonics, and therefore the following discussion is based on the results of the stationary phase method.

4. Condition and regimes

a. Condition for frequency change

Because the change in intrinsic frequency arises from the Doppler shift as indicated by (3.2), the extent of the frequency change can be estimated from

$$\frac{2k_b U_i}{\omega_i}, \tag{4.1}$$

where $2U_i$ is the amplitude of the horizontal flow that is parallel to the topographic wavenumber vector and is associated with the incident and primary reflected waves at the bottom. The frequency change is significant when this ratio is on the order of, or much greater than, unity.

It is noteworthy that this condition for frequency change can be satisfied in a realistic parameter range. For example, consider an incident wave of a semidiurnal tidal frequency with a flow amplitude of 5 cm s^{-1}; in that case, the topographic wavelength $2\pi/k_b$ required is approximately 4 km when $2k_bU_i/\omega_i = 1$ (and hence $\omega_s \sim \omega_i$) or approximately 400 m when $2k_bU_i/\omega_i = 10$ (and hence $\omega_s \gg \omega_i$). These estimates suggest that the occurrence of scattering with frequency change could be a common phenomenon in the ocean because the bottom roughness of such scales is widely distributed in the oceans.

More precisely, the horizontal wavenumber of scattered waves is the sum and difference of the horizontal wavenumbers of the incident wave and the topography (i.e., $\mathbf{k}_s^h = \mathbf{k}_i^h + \mathbf{k}_b$; Baines 1971a), although the horizontal wavenumber of the scattered waves is approximated as that of the topography in the above [i.e., $k_s \approx (\theta_b k_b =) \pm k_b$] through the assumption that the incident wave is slowly varying relative to the scattered waves (i.e., $|\mathbf{k}_i^h|/|\mathbf{k}_b| \approx 0$). Then the more precise measure of the frequency change may be given by

$$\frac{|\mathbf{k}_s^h \cdot \mathbf{u}_{i+r}^h|}{\omega_i}, \tag{4.2}$$

where the superscript h the horizontal component.

b. Parameter regimes of frequency change

The ratio (4.2) implies the presence of the following three regimes:

(i) $|\mathbf{k}_s^h \cdot \mathbf{u}_{i+r}^h|/\omega_i \gg 1$: The scattered wave frequency is much greater than the incident-wave frequency.

(ii) $|\mathbf{k}_s^h \cdot \mathbf{u}_{i+r}^h|/\omega_i \sim 1$: The scattered wave frequency is on the order of, or much smaller than, the incident-wave frequency.

(iii) $|\mathbf{k}_s^h \cdot \mathbf{u}_{i+r}^h|/\omega_i \ll 1$: The scattered wave frequency is almost equal to the incident-wave frequency.

The regimes (i)–(iii) correspond to the regimes in which quasi-steady lee waves, mixed tidal-lee (MTL) waves, and internal tides are generated by a barotropic tidal flow, respectively (Nakamura et al. 2000). Frequency conservation is not valid in the first two regimes, but it provides a good approximation in the last regime, which has been considered in the previous studies.

The parameter regimes can be also viewed in terms of horizontal scale. Frequency change occurs when the topography is sufficiently rough because the ratio (4.2) can be approximated as that of the flow excursion at the bottom ($|\mathbf{u}_{i+r}^h|/\omega_i$) to the topographic length scale ($|\mathbf{k}_b|^{-1}$). This roughness of the topography is reflected by the difference in scale between the horizontal wavenumbers of incident and scattered waves. Denoting these wavenumbers as K_i and K_s ($=|\mathbf{k}_i^h + \mathbf{k}_b|$), respectively, we can scale the ratio (4.2) as

$$\frac{|(\mathbf{k}_i^h + \mathbf{k}_b) \cdot \mathbf{u}_{i+r}^h|}{\omega_i} \sim \frac{K_s U_{i+r}}{\omega_i} = \left(\frac{K_s}{K_i}\right)\left(\frac{K_i U_{i+r}}{\omega_i}\right), \quad (4.3)$$

where $U_{i+r} = |\mathbf{u}_{i+r}^h|$. Here, the ratio in the last bracket,

$$\Delta = \frac{K_i U_{i+r}}{\omega_i}, \quad (4.4)$$

is the wave Froude number (or temporal Rossby number) of the incident and primary reflected waves.

Using Δ and K_i/K_s, the extent of frequency change on scattering can be estimated as follows (also shown in Fig. 1):

1) $K_s U_{i+r}/\omega_i \sim 1$ when $K_i/K_s \ll 1$ and $\Delta \ll 1$
   Significant frequency change occurs (the MTL wave regime) when the horizontal wavenumber of the topography is much higher than that of the incident wave, even if the incident and primary reflected waves are approximately linear.
2) $K_s U_{i+r}/\omega_i \gg 1$ when $K_i/K_s \ll \delta' \ll 1$ and $\Delta \ll 1$ (where δ' is a small parameter)
   The scattered wave frequency is much higher than the incident-wave frequency (the lee-wave regime) when the horizontal wavenumber of the topography is higher than that of the incident wave by more than two orders, if the incident and primary reflected waves are approximately linear.
3) $K_s U_{i+r}/\omega_i \sim 1$ when $K_i/K_s \sim 1$ and $\Delta \sim 1$
   When the incident and primary reflected waves are highly nonlinear, frequency change is significant (the MTL wave regime), even if the topographic wavenumber is on the order of the incident-wave wavenumber.
4) $K_s U_{i+r}/\omega_i \gg 1$ when $K_i/K_s \ll 1$ and $\Delta \sim 1$
   When the incident and primary reflected waves are highly nonlinear, a much lower topographic wavenumber is sufficient to make the scattered wave frequency much higher than the incident-wave frequency (the lee-wave regime).
5) $K_s U_{i+r}/\omega_i \ll 1$ when $K_i/K_s \sim 1$ and $\Delta \ll 1$
   Frequency change hardly occurs (the internal tide regime) when the horizontal wavenumber of the topography is on the order of that of the incident wave, if the incident and primary reflected waves are approximately linear. In this regime, the linear scattering considered in the previous studies occurs.
6) $K_s U_{i+r}/\omega_i \ll 1$ when $K_i/K_s \gg 1$
   Reflection rather than scattering occurs.

Hence, the scattered waves have much higher horizontal wavenumbers than the incident wave when the frequency change occurs, except for case 3. In cases 1, 2, and 4, the corresponding topographic wavenumber K_b is almost equal to the horizontal wavenumber of the scattered waves (K_s) because the topography is very rough compared to the wavelength of the incident wave. Note that the wave Froude number Δ should not be greater than unity because this would be unphysical—the incident wave would break. This parameter range is excluded from the above list.

5. Derivation of leading-order equations for scattered waves in various regimes

The discussion has hitherto been based on the governing Eqs. (2.1) and the boundary condition (2.3), assuming that the spatial derivative of the primary wave field is negligible. However, as shown in the previous section, there are several parameter regimes in which frequency change occurs, and the difference between spatial or temporal scales of the primary and scattered waves varies among these regimes. Also, the consideration of the effect of the advection by the primary waves implicitly assumes that the incident wave has finite amplitude. It is therefore required to know which terms can be neglected in what regime and the resulting error. To discuss these issues, we present a more rigorous derivation that leads to different governing equations for different regimes, as will be shown in section 5c.

a. Scaling 1: Separation of the scattered wave field

To derive the appropriate governing equations, we first isolate the scattered wave field from the total wave

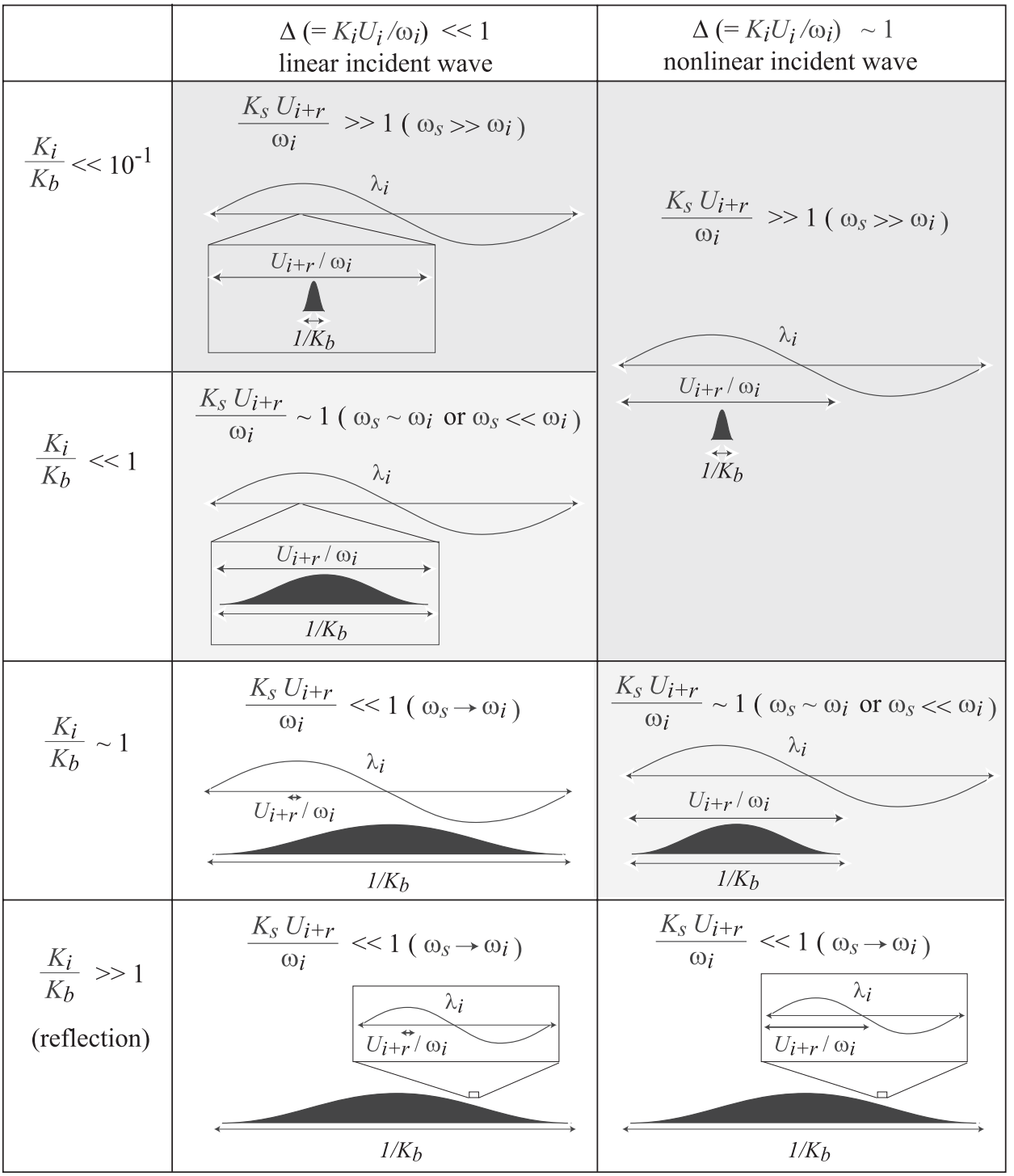

FIG. 1. Diagram of the parameter regimes of K_sU_{i+r}/ω_i, which is a measure of the change in scattered wave frequency, as functions of the length scale of topography with respect to that of incident wave (K_i/K_b) and the wave Froude number of an incident wave ($\Delta = K_iU_i/\omega_i$). Here, K, U, and ω are the horizontal wavenumber, current amplitude, and frequency, respectively. The subscripts s, i, $i + r$, and b denote scattered, incident, incident and primary reflected waves, and bottom topography, respectively. Also shown are scales of the bottom topography (K_b^{-1}), current excursion of incident and primary reflected waves (U_{i+r}/ω_i), and incident-wave wavelength (λ_i). Significant frequency change occurs in the shaded regimes. Note that $K_b \sim K_s$ when $K_i/K_b \sim 1$ or $\ll 1$.

field in this subsection in order to derive equations for scattered waves through a scaling argument in subsequent subsections.

1) GOVERNING EQUATIONS OF THE TOTAL FIELD

As in the previous sections, we consider the reflection of a monochromatic internal wave over small-amplitude bottom topography. Although the discussion here is limited to the topography with no mean slope, it can be easily extended to the case with a mean slope. The equations for an inviscid, rotating, and uniformly stratified Boussinesq fluid are

$$\begin{aligned} \frac{\partial \mathbf{u}}{\partial t} + (\mathbf{u}\cdot\nabla)\mathbf{u} + f\mathbf{z}\times\mathbf{u} &= -\frac{\nabla p}{\rho_0} - \frac{\rho' g}{\rho_0}\mathbf{z}, \\ \nabla\cdot\mathbf{u} &= 0, \\ \frac{\partial \rho'}{\partial t} + \mathbf{u}\cdot\nabla\rho' + w\frac{\partial \overline{\rho}}{\partial z} &= 0, \end{aligned} \tag{5.1}$$

where standard notations are used and $\mathbf{z}$ is a unit vector in the vertical direction. The density is separated into a reference value, background stratification, and perturbation as in (2.4), and the hydrostatic balance for a resting fluid is subtracted from the momentum equation. The kinematic boundary condition at the bottom is

$$w = \mathbf{u}^h\cdot\nabla^h h = 0 \quad \text{at } z = h(\mathbf{x}^h). \tag{5.2}$$

The governing equations retain the advection terms to consider the effects of the background flow on scattered waves; thus, they cannot be solved in their original form. To transform these equations into a tractable yet relevant form, we define the scattered wave field in a manner in which it is convenient to apply the multiple scale method.

2) DEFINITION OF SCATTERED WAVE FIELD

As noted in section 2, the total reflected wave field comprises the primary reflected waves on the order of ϵ^0 and scattered waves on higher orders (e.g., Müller and Xu 1992), where ϵ is a nondimensional scale of topographic height; its precise definition in this study is given in (5.24) or appendix B. Also, the sum of the incident and primary reflected waves is identical to the solution for reflection on a plane.

Based on these facts, we define the scattered wave field as the difference between the solution for reflection on a rough topography and that on a plane; that is,

$$\text{(scattered)} \underline{\underline{\text{def}}} \text{(total)} - \text{(reflection on a plane)}. \tag{5.3}$$

This roughly corresponds to an expansion of the wave field with respect to ϵ. This definition isolates the scattered wave field and thus it is helpful for the scaling of the governing equations in section 5b. In this definition, the results of the nonlinearity of incident and primary reflected waves are excluded, whereas nonlinear interactions involving scattered waves are all included in the scattered wave field. This enables a clear separation of scattered waves from incident and primary reflected waves of higher orders (or higher harmonics) and thus simplifies the treatment of incident waves. Nevertheless, it should be noted that the definition (5.3) can be unimportant for the case $\Delta \ll 1$ in which nonlinear terms are neglected in the leading order and the spatial scale of incident and scattered waves differs greatly, as shown in Fig. 1.

3) MULTIPLE SCALE METHOD

The discussion in section 4 indicates that when the frequency change occurs, the horizontal wavenumber of the scattered waves is generally much higher than that of the incident and primary reflected waves because Δ should not be greater than unity. We thus utilize the method of multiple scales by separating the wave field into large- and small-scale fields. The large-scale field is scaled by the incident-wave frequency and wavenumbers (which are the same as those of the primary reflected waves), whereas the small-scale filed is scaled by those of the scattered waves, as given by

$$\begin{aligned} \frac{\partial}{\partial t} &= \omega_s\frac{\partial}{\partial \tilde{t}_s} + \omega_l\frac{\partial}{\partial \tilde{t}_l}, \\ \frac{\partial}{\partial x} &= k_s\frac{\partial}{\partial \tilde{x}_s} + k_l\frac{\partial}{\partial \tilde{x}_l}, \\ \frac{\partial}{\partial z} &= m_s\frac{\partial}{\partial \tilde{z}_s} + m_l\frac{\partial}{\partial \tilde{z}_l}, \end{aligned} \tag{5.4}$$

where the large and small scales are denoted by the subscripts l and s, respectively, and where $\tilde{}$ denotes nondimensional variables.

Then, dependent variables are separated into those for the large and small scales and are scaled as

$$\begin{aligned} (u,v,w) &= (U_l\tilde{u}_l, V_l\tilde{v}_l, W_l\tilde{w}_l) + (U_s\tilde{u}_s, V_s\tilde{v}_s, W_s\tilde{w}_s) \\ p &= P_l\tilde{p}_l + P_s\tilde{p}_s, \\ \rho' &= R_l\tilde{\rho}'_l + R_s\tilde{\rho}'_s. \end{aligned} \tag{5.5}$$

Note that the large-scale variables are functions of only x_l, z_l, and t_l, such as

$$\begin{aligned} u_l &= U_l\tilde{u}_l(x_l, z_l, t_l), \\ u_s &= U_s\tilde{u}_s(x_s, z_s, t_s; x_l, z_l, t_l). \end{aligned} \tag{5.6}$$

This is because nonlinear interactions do not occur between a monochromatic incident wave and the primary reflected wave over a horizontal plane. In the case of sloping topography or nonmonochromatic incident

waves such as tidal beams, nonlinear interactions can generate higher harmonics (e.g., Thorpe 1997; Lamb 2004). Nevertheless, these higher harmonics can be neglected when $\Delta \ll 1$ as long as a resonant interaction does not occur; without resonance, the higher harmonics are of higher orders of magnitude with respect to Δ. If needed, the inclusion of such effects is possible owing to the definition (5.3).

For simplicity, we consider the bottom topography with a single small length scale of $1/k_s$, namely,

$$h = H\tilde{h}(x_s). \tag{5.7}$$

We do so because the frequency change is insignificant when the topography varies only on a large scale [i.e., $h = h(x_l)$], except for case 3 in section 4b. Further, the scattering off topography with various length scales can be obtained to the leading order by the superposition of the waves scattered off each topographic Fourier component for small-amplitude topography.

4) RATIOS OF THE SCALES

The multiple scale method yields three ratios of scales:

$$\delta_\omega = \frac{\omega_l}{\omega_s}, \quad \delta_k = \frac{k_l}{k_s}, \quad \delta_m = \frac{m_l}{m_s}. \tag{5.8}$$

Each ratio must be much smaller or much larger than unity for the multiple scale method to be applicable to the corresponding direction (or time). We thus examine the scales of these ratios.

To scale the ratios, we utilize the dispersion relation and the condition for frequency change. The dispersion relation of linear internal waves can be approximated as $\omega \simeq Nk/m$ if $f \ll \omega \ll N$, where N is the buoyancy frequency. The above three ratios are therefore related to each other by

$$\delta_\omega \sim \frac{\delta_k}{\delta_m} \tag{5.9}$$

when the condition $f \ll \omega \ll N$ is satisfied for both ω_s and ω_l. (The cases $\omega \sim f$ and $\omega \sim N$ are discussed in appendix A.)

In section 4, we found that the condition for frequency change requires

$$\frac{k_s U_l}{\omega_l} \gg 1 \quad \text{or} \quad \sim 1. \tag{5.10}$$

The nondimensional parameter $k_s U_l/\omega_l$ corresponds to the ratio (4.2) and thus the former regime ($k_s U_l/\omega_l \gg 1$) corresponds to the lee-wave regimes 2 and 4 in section 4b, whereas the latter ($k_s U_l/\omega_l \sim 1$) corresponds to the MTL wave regimes 1 and 3. This parameter can be rearranged as

$$\frac{k_s U_l}{\omega_l} = \left(\frac{k_s}{k_l}\right)\left(\frac{k_l U_l}{\omega_l}\right) \sim \frac{\Delta}{\delta_k}, \tag{5.11}$$

where Δ ($= k_l U_l/\omega_l$), which is redefined here and corresponds to (4.4), is now the wave Froude number (or temporal Rossby number) of the large-scale waves and is thus the measure of their nonlinearity. (Note that Δ takes, in general, various values from infinitely small values for infinitesimal waves to around unity for highly nonlinear waves, and it cannot be specified unless the incoming wave is specified.)

When $k_s U_l/\omega_l \gg 1$, it follows that $\omega_s \gg \omega_l$. This is because in this parameter regime, the scattered wave frequency is almost equal to the lee-wave frequency, which can be scaled as $\omega_s \sim k_s U_l$; thus,

$$\delta_\omega = \frac{\omega_l}{\omega_s} \sim \left(\frac{k_s U_l}{\omega_l}\right)^{-1}. \tag{5.12}$$

Note that the last term is much smaller than unity in this regime. The combination of (5.9), (5.11), and (5.12) yields

$$\delta_\omega \sim \delta, \quad \delta_k \sim \delta\Delta, \quad \delta_m \sim \Delta. \tag{5.13}$$

Here, we define a small parameter δ as $\delta = \delta_\omega$. The parameter δ will be used later to represent the "small parameters" arising from the multiple scale method (i.e., δ_ω, δ_k, and δ_m) by a single parameter.

When $k_s U_l/\omega_l \sim 1$, two cases are possible: $\omega_s \sim \omega_l$ and $\omega_s \ll \omega_l$. In the former case ($\omega_s \sim \omega_l$), ω_s is still on the order of $k_s U_l$ and thus (5.12) holds in a similar manner. Therefore, the use of (5.9), (5.11), and (5.12) yields

$$\delta_\omega \sim 1, \quad \delta_k \sim \delta_m \sim \delta \sim \Delta, \tag{5.14}$$

where we define $\delta = \delta_k$ because δ_ω ($= \omega_l/\omega_s$) ~ 1.

The latter case ($\omega_s \ll \omega_l$) arises when the Doppler shift is almost equal to the incident-wave frequency and thus their difference, which is equal to the scattered-wave frequency under consideration, becomes much smaller than the incident-wave frequency. In this case, (5.12) does not hold because

$$\omega_s \ll \omega_l \sim k_s U_l. \tag{5.15}$$

Using (5.15) instead of (5.12) and defining $\delta = \delta_\omega^{-1}$, we obtain the following from (5.9) and (5.11):

$$\delta_\omega \sim \delta^{-1}, \quad \delta_k \sim \Delta, \quad \delta_m \sim \delta\Delta. \tag{5.16}$$

The above scales of the three ratios are summarized in Table 1. It is apparent that the multiple scale method is

TABLE 1. Scales of δ_ω, δ_k, and δ_m. The ratio δ_ϕ is defined as ϕ_l/ϕ_s where subscripts l and s indicate large and small scales. In the regimes $\omega_s \gg \omega_l$ and $\omega_s \ll \omega_l$, the relation between δ and Δ is situation dependent. Once the incident wave and bottom topography are given, we may write $\delta^n \sim \Delta$, for $\Delta \ll 1$, where n is a natural number when $\delta \geq \Delta$ or the inverse of a natural number when $\delta \leq \Delta$.

Regime	$k_sU_l/\omega_l \gg 1$	$k_sU_l/\omega_l \sim 1$	
Intrinsic frequency	$\omega_s \gg \omega_l$	$\omega_s \sim \omega_l$	$\omega_s \ll \omega_l$
Scales of ratios in terms of δ, Δ	$\delta_\omega\ (\ll 1) = \delta$	$\delta_\omega \sim 1$	$\delta_\omega^{-1}(\ll 1) = \delta$
	$\delta_k \sim \delta\Delta$	$\delta_k = \delta \sim \Delta$	$\delta_k \sim \Delta$
	$\delta_m \sim \Delta$	$\delta_m \sim \delta$	$\delta_m \sim \delta\Delta$
when $\Delta \ll 1$ ($\Delta \sim \delta^n$)	$\delta_\omega\ (\ll 1) = \delta$	$\delta_\omega \sim 1$	$\delta_\omega^{-1}(\ll 1) = \delta$
	$\delta_k \sim \delta^{n+1} \ll 1$	$\delta_k = \delta \ll 1$	$\delta_k \sim \delta^n \ll 1$
	$\delta_m \sim \delta^n \ll 1$	$\delta_m \sim \delta \ll 1$	$\delta_m \sim \delta^{n+1} \ll 1$
when $\Delta \sim 1$	$\delta_\omega\ (\ll 1) = \delta \sim \delta_k$	$\delta_\omega \sim \delta_k \sim \delta_m \sim 1$	$\delta_\omega^{-1}(\ll 1) = \delta \sim \delta_m$
	$\delta_m \sim 1$		$\delta_k \sim 1$

applicable in most cases. In the linear case $\Delta \ll 1$, it is applicable to all the directions and time, except for the case $\omega_s \sim \omega_l$, in which it is inapplicable to time. Even in the nonlinear case $\Delta \sim 1$, the multiple scale method is applicable to the t and x directions in the lee-wave regime ($\omega_s \gg \omega_l$) and to the t and z directions in the case $\omega_s \ll \omega_l$.

It would be useful if these scales of δ_ω, δ_k, and δ_m were written in terms of δ alone so that the governing equations for the higher-order scattered waves could be systematically obtained if desired. To do so, Δ should be written in terms of δ, when $\Delta \ll 1$ (it is unnecessary when $\Delta \sim 1$ because the order of magnitude of Δ is already given).

In the regime $\omega_s \sim \omega_l$, (5.14) indicates that $\delta \sim \Delta$. In the other two regimes, there is no general relation between δ and Δ because Δ depends on the properties of an incident wave, whereas δ is determined by both the topographic wavenumber and the flow excursion of the incident wave ($2U_i/\omega_i$, where $2U_i = U_{i+r}$). Nevertheless, once the incident wave and topography are given, the magnitudes of both Δ and δ become known values. Then, this specific value of Δ may be written using the specific value of δ as, for example,

$$\Delta \sim \delta^n. \tag{5.17}$$

Here, n is a natural number (if $\delta \geq \Delta$) or the inverse of a natural number (if $\delta \leq \Delta$). The value of n should be determined according to the situation under consideration. The results of the substitution are shown in Table 1. On the other hand, the results become significantly simpler when $\Delta \sim 1$, as also shown in Table 1.

b. Scaling 2: Nondimensional equations

By separating the scattered wave field from the total and using the scales described in section 5a(3), we nondimensionalize the equations of the large- and small-scale fields. The multiple scale method is formally applied to t, x, and z in order to derive nondimensional equations that are useful for various parameter regimes. The applicability of the multiple scale method will be taken into consideration after the nondimensional equations are obtained.

1) LARGE SCALE

From definition (5.3), the large-scale wave field satisfies the original governing equations even without scattered waves. Also, the large-scale wave field varies only on the large scale, as noted in (5.6).

The continuity equation thus becomes

$$(k_lU_l)\frac{\partial \tilde{u}_l}{\partial \tilde{x}_l} + (m_lW_l)\frac{\partial \tilde{w}_l}{\partial \tilde{z}_l} = 0 \tag{5.18}$$

and hence

$$k_lU_l \sim m_lW_l. \tag{5.19}$$

The nondimensional momentum equations are obtained similarly. We divide the equations by the scale of each local temporal change term (instead of the Coriolis term used in the derivation of quasigeostrophic equations, since the motion being considered comprises propagating internal waves). Using (5.19), it follows that

$$\begin{aligned}
&\frac{\partial \tilde{u}_l}{\partial \tilde{t}_l} + \Delta\left(\tilde{u}_l\frac{\partial \tilde{u}_l}{\partial \tilde{x}_l} + \tilde{w}_l\frac{\partial \tilde{u}_l}{\partial \tilde{z}_l}\right) - \left(\frac{f^2}{\omega_l^2}\right)\tilde{v}_l = -\frac{\partial \tilde{p}_l}{\partial \tilde{x}_l},\\
&\frac{\partial \tilde{v}_l}{\partial \tilde{t}_l} + \Delta\left(\tilde{u}_l\frac{\partial \tilde{v}_l}{\partial \tilde{x}_l} + \tilde{w}_l\frac{\partial \tilde{v}_l}{\partial \tilde{z}_l}\right) + \tilde{u}_l = 0,\\
&\left(\frac{k_l^2}{m_l^2}\right)\left[\frac{\partial \tilde{w}_l}{\partial \tilde{t}_l} + \Delta\left(\tilde{u}_l\frac{\partial \tilde{w}_l}{\partial \tilde{x}_l} + \tilde{w}_l\frac{\partial \tilde{w}_l}{\partial \tilde{z}_l}\right)\right] = -\frac{\partial \tilde{p}_l}{\partial \tilde{z}_l} - \tilde{\rho}_l'.
\end{aligned} \tag{5.20}$$

In the derivation, we performed the scalings $P_l \sim \rho_0\omega_lU_l/k_l$, $R_l \sim m_lP_l/g$, and $V_l \sim (f/\omega_l)U_l$. The first implies that the horizontal pressure gradient term is on the order of the local temporal change term, since both terms are fundamental to internal wave dynamics. The second

implies that the gravity acceleration term is on the order of the vertical pressure gradient term (i.e., the hydrostatic balance is significant). The last one is for convenience and is valid when $\omega_l \sim f$. In the other case, the Coriolis term is automatically neglected using this form (because the case $\omega_l < f$ is not considered).

Similarly, the density equation becomes

$$\frac{\partial \tilde{\rho}_l'}{\partial \tilde{t}_l} + \Delta\left(\tilde{u}_l \frac{\partial \tilde{\rho}_l'}{\partial \tilde{x}_l} + \tilde{w}_l \frac{\partial \tilde{\rho}_l'}{\partial \tilde{z}_l}\right) = -\left(\frac{k_l^2}{m_l^2}\frac{N^2}{\omega_l^2}\right)\tilde{w}_l, \quad (5.21)$$

where $N = [-(g/\rho_0)(d\overline{\rho}/dz)]^{1/2}$. Note that the coefficient of the right-hand side is $O(1)$, as obtained from the hydrostatic dispersion relation ($\omega \simeq Nk/m$).

The bottom boundary condition for the large-scale waves is given as $\tilde{w}_l = 0$ at $\tilde{z} = 0$, since these waves comprise the incident and reflected waves on a horizontal plane.

2) SMALL SCALE

Nondimensional equations of the small-scale waves are obtained from the use of the multiple scale method (5.4) to (5.6) and the subtraction of the corresponding large-scale equation.

(i) Continuity equation

A nondimensional continuity equation for the small scale is obtained as

$$\frac{\partial \tilde{u}_s}{\partial \tilde{x}_s} + \delta_k \frac{\partial \tilde{u}_s}{\partial \tilde{x}_l} + \left(\frac{m_s W_s}{k_s U_s}\right)\left(\frac{\partial \tilde{w}_s}{\partial \tilde{z}_s} + \delta_m \frac{\partial \tilde{w}_s}{\partial \tilde{z}_l}\right) = 0, \quad (5.22)$$

when scaled by $k_s U_s$ after the subtraction of the large-scale continuity Eq. (5.18). Because both δ_k and δ_m are much less than unity as long as $\Delta \ll 1$ (Table 1), the third term in (5.22) must be $O(1)$; hence,

$$k_s U_s \sim m_s W_s. \quad (5.23)$$

When $\Delta \sim 1$, δ_k or δ_m (or both) is $O(1)$ and thus the multiple scale method is not applicable along the corresponding direction. Even in such a case, (5.23) is valid as the scaling for leading-order scattered waves whose wavenumber is scaled as $k_s \sim k_l$ or $m_s \sim m_l$ (or both).

(ii) Bottom boundary condition

The assumption of small-amplitude topography comprises two conditions: (i) the height of the topography is smaller than the vertical scale of the waves under consideration and (ii) the slope of the topography is smaller than the wave slope. These conditions are satisfied, as argued in appendix B, when

$$\epsilon = Hm_s \ll 1 \,(\text{and}\, \epsilon \lesssim \delta \text{ when } \delta_\omega \ll 1), \quad (5.24)$$

where ϵ is the nondimensional topographic height scale used in this study. Under this condition, the bottom boundary condition (5.2) can be expanded around $z = 0$ as

$$w - \nabla^h \cdot (h\mathbf{u}^h) - \nabla^h \cdot \left(\frac{1}{2}h^2 \frac{\partial \mathbf{u}^h}{\partial z}\right) - \cdots = 0 \quad \text{at } z = 0, \quad (5.25)$$

following Müller and Xu (1992).

Noting that $h = h(x_s)$ and $w_l = 0$ at $z = 0$, the nondimensional bottom boundary condition, which is scaled by W_s, becomes

$$\tilde{w}_s(z=0) = \left(\frac{k_s U_l H}{W_s}\right)\left[\left(\tilde{u}_l + \left(\frac{U_s}{U_l}\right)\tilde{u}_s\right)\frac{\partial \tilde{h}}{\partial \tilde{x}_s} + \left(\frac{U_s}{U_l}\right)\tilde{h}\frac{\partial \tilde{u}_s}{\partial \tilde{x}_s} + \delta_k \tilde{h}\left(\frac{\partial \tilde{u}_l}{\partial \tilde{x}_l} + \left(\frac{U_s}{U_l}\right)\frac{\partial \tilde{u}_s}{\partial \tilde{x}_l}\right)\right] + (O(\epsilon)). \quad (5.26)$$

The condition that the scale of the leading-order terms on both sides be the same gives

$$1 \sim \frac{k_s U_l H}{W_s} \sim Hm_s\left(\frac{U_s}{U_l}\right)^{-1}, \quad (5.27)$$

using (5.23). It follows that

$$\epsilon \sim \frac{U_s}{U_l}. \quad (5.28)$$

This relation should be emphasized. The bottom boundary condition relates the topographic height scale to the ratio of the amplitudes of the incident and scattered waves (or the large and small scales). The relation is common to the case of linear steady lee waves (cf. Baines 1995) and suggests that $U_s/U_l \ll 1$ for small-amplitude topography, which satisfies (5.24).

The nondimensional boundary condition can be rearranged using (5.27) as

$$\tilde{w}_s(z=0) = \tilde{u}_l \frac{\partial \tilde{h}}{\partial \tilde{x}_s} + \delta_k\left(\tilde{h}\frac{\partial \tilde{u}_l}{\partial \tilde{x}_l}\right) + \epsilon\left\{\tilde{u}_s \frac{\partial \tilde{h}}{\partial \tilde{x}_s} + \frac{\partial \tilde{u}_s}{\partial \tilde{x}_s}\tilde{h} + \delta_k\left(\tilde{h}\frac{\partial \tilde{u}_s}{\partial \tilde{x}_l}\right) + \delta_m\left[\tilde{h}\frac{\partial \tilde{h}}{\partial \tilde{x}_s}\frac{\partial \tilde{u}_l}{\partial \tilde{z}_l} + \frac{1}{2}\delta_k\left(\tilde{h}^2\frac{\partial^2 \tilde{u}_s}{\partial \tilde{x}_s \partial \tilde{z}_s}\right)\right]\right\} + [O(\epsilon^2)], \quad (5.29)$$

where the terms of the next order in ϵ are also written.

It is interesting that the order of each term depends not only on ϵ but also on δ_k and δ_m. This suggests that the relative magnitude of these three nondimensional parameters must be specified to obtain scattered waves

of various orders. For example, when $\delta_k \sim \epsilon\ (\lesssim \delta_m)$, the effect of the spatial variation of an incident wave ($\tilde{h}\partial\tilde{u}_l/\partial\tilde{x}_l$) is excluded from the leading order and is included in the second-order scattered waves, which also include the scattering of the leading-order scattered waves ($\tilde{u}_s\partial\tilde{h}/\partial\tilde{x}_s + \partial\tilde{u}_s/\partial\tilde{x}_s\tilde{h}$). This point has not been considered in the previous studies.

(iii) Momentum and density equations

The nondimensional momentum equations for the small scale, which are scaled by the corresponding local temporal change terms, are rearranged using (5.19), (5.23), and (5.28) to give

$$\begin{aligned}
&\frac{D\tilde{u}_s}{Dt} + \left(\frac{k_sU_l}{\omega_s}\right)\left[\delta_k\tilde{u}_s\frac{\partial\tilde{u}_l}{\partial\tilde{x}_l} + \delta_m\tilde{w}_s\frac{\partial\tilde{u}_l}{\partial\tilde{z}_l}\right] - \left(\frac{f^2}{\omega_s^2}\right)\tilde{v}_s \\
&\qquad = -\left(\frac{\partial\tilde{p}_s}{\partial\tilde{x}_s} + \delta_k\frac{\partial\tilde{p}_s}{\partial\tilde{x}_l}\right), \\
&\frac{D\tilde{v}_s}{Dt} + \left(\frac{k_sU_l}{\omega_s}\right)\left[\frac{\delta_k}{\delta_\omega}\tilde{u}_s\frac{\partial\tilde{v}_l}{\partial\tilde{x}_l} + \frac{\delta_m}{\delta_\omega}\tilde{w}_s\frac{\partial\tilde{v}_l}{\partial\tilde{z}_l}\right] + \tilde{u}_s = 0, \\
&\frac{D\tilde{w}_s}{Dt} + \left(\frac{k_sU_l}{\omega_s}\right)\left[\frac{\delta_k^2}{\delta_m}\tilde{u}_s\frac{\partial\tilde{w}_l}{\partial\tilde{x}_l} + \delta_k\tilde{w}_s\frac{\partial\tilde{w}_l}{\partial\tilde{z}_l}\right] \\
&\qquad = -\left(\frac{m_s^2}{k_s^2}\right)\left[\left(\frac{\partial\tilde{p}_s}{\partial\tilde{z}_s} + \delta_m\frac{\partial\tilde{p}_s}{\partial\tilde{z}_l}\right) + \tilde{\rho}_s'\right],
\end{aligned} \tag{5.30}$$

where

$$\begin{aligned}
\frac{D}{Dt} = &\frac{\partial}{\partial\tilde{t}_s} + \delta_\omega\frac{\partial}{\partial\tilde{t}_l} \\
&+ \left(\frac{k_sU_l}{\omega_s}\right)\left[(\tilde{u}_l + \epsilon\tilde{u}_s)\left(\frac{\partial}{\partial\tilde{x}_s} + \delta_k\frac{\partial}{\partial\tilde{x}_l}\right)\right. \\
&\left.+ \left(\frac{\delta_k}{\delta_m}\right)\left(\tilde{w}_l + \left(\epsilon\frac{\delta_m}{\delta_k}\right)\tilde{w}_s\right)\left(\frac{\partial}{\partial\tilde{z}_s} + \delta_m\frac{\partial}{\partial\tilde{z}_l}\right)\right].
\end{aligned} \tag{5.31}$$

Similar to the derivation of the large-scale equations, we used the scalings $P_s \sim \rho_0\omega_sU_s/k_s$, $R_s \sim m_sP_s/g$, and $V_s \sim (f/\omega_s)U_s$.

Similarly, the density equation is nondimensionalized as

$$\begin{aligned}
&\frac{D\tilde{\rho}_s'}{Dt} + \left(\frac{k_sU_l}{\omega_s}\right)\left[(\delta_\omega\delta_m)\tilde{u}_s\frac{\partial\tilde{\rho}_l'}{\partial\tilde{x}_l} + \frac{\delta_\omega\delta_m^2}{\delta_k}\tilde{w}_s\frac{\partial\tilde{\rho}_l'}{\partial\tilde{z}_l}\right] \\
&\qquad = -\left(\frac{k_s^2}{m_s^2}\frac{N^2}{\omega_s^2}\right)\tilde{w}_s.
\end{aligned} \tag{5.32}$$

c. Scaling 3: Leading-order equations

Using the above nondimensional equations and parameters, which are derived without any assumptions about Δ or δ except that $\Delta < 1$, this section shows the leading-order equations in Δ for the large scale, presents the method to obtain equations of various orders in δ for the small scale, and shows the leading-order equations for various regimes.

1) LARGE SCALE

To allow a linear approximation for the large-scale waves, we consider the case $\Delta \ll 1$ and expand the large-scale variables with respect to Δ, as given by

$$u_l = u_l^{(0)} + \Delta u_l^{(1)} + \cdots. \tag{5.33}$$

The substitution of (5.33) into (5.20) and (5.21) and the rearrangement with respect to Δ yields large-scale equations of various orders. The leading-order equations (i.e., the zeroth order in Δ) are

$$\begin{aligned}
&\frac{\partial\tilde{u}_l^{(0)}}{\partial\tilde{t}_l} - \left(\frac{f^2}{\omega_l^2}\right)\tilde{v}_l^{(0)} = -\frac{\partial\tilde{p}_l^{(0)}}{\partial\tilde{x}_l}, \\
&\frac{\partial\tilde{v}_l^{(0)}}{\partial\tilde{t}_l} + \tilde{u}_l^{(0)} = 0, \\
&\left(\frac{k_l^2}{m_l^2}\right)\frac{\partial\tilde{w}_l^{(0)}}{\partial\tilde{t}_l} = -\frac{\partial\tilde{p}_l^{(0)}}{\partial\tilde{z}_l} - \tilde{\rho}_l'^{(0)}, \\
&\frac{\partial\tilde{\rho}_l'^{(0)}}{\partial\tilde{t}_l} = -\left(\frac{k_l^2}{m_l^2}\frac{N^2}{\omega_l^2}\right)\tilde{w}_l^{(0)}, \\
&\frac{\partial\tilde{u}_l^{(0)}}{\partial\tilde{x}_l} + \frac{\partial\tilde{w}_l^{(0)}}{\partial\tilde{z}_l} = 0.
\end{aligned} \tag{5.34}$$

These are the governing equations of the primary waves used in section 2. Higher-order equations, which are required to consider the higher-order scattered waves, can be obtained similarly, although these are omitted for conciseness.

Note that if we consider monochromatic incident waves, sinusoidal solutions are possible even if $\Delta \sim 1$ for the Boussinesq fluid of a constant buoyancy frequency. Even in this case, the equations for the small-scale field can be obtained by the method described in the next section. In other words, taking into consideration the effects of advection by the primary waves is possible even for approximately linear primary waves in certain parameter ranges. This enables us to extend the results obtained in this study to a case with a mean slope, a case for polychromatic incident waves, and so on.

2) SMALL SCALES

Small-scale equations and the bottom boundary condition in the various regimes and of various orders in δ can be systematically obtained using the following procedure: (i) represent the parameters δ_ω, δ_k, and δ_m in terms of δ for each regime, as indicated in Table 1; (ii) if

TABLE 2. Leading-order equations. The scattered wave equations to the zeroth order in both ϵ and δ (or Δ for the case $k_s U_l/\omega_l \ll 1$). The equations in the regime $k_s U_l/\omega_l \sim 1$ and $\omega_s \ll \omega_l$ are omitted. Note that $U_l = U_{i+r} = 2U_i$ for a monochromatic incident wave. The definitions of ϵ, δ, and Δ are provided in (5.24) and in section 5a(4).

$\Delta \ll 1$

$\omega_s \gg \omega_l$ (i.e., $k_s U_l/\omega_l \gg 1$), $\delta \sim \Delta$	$\omega_s \sim \omega_l$ (i.e., $k_s U_l/\omega_l \sim 1$)	$\omega_s \to \omega_l$ (i.e., $k_s U_l/\omega_l \ll 1$)
$\dfrac{D\tilde{u}_s^{(0)}}{Dt} = -\dfrac{\partial \tilde{p}_s^{(0)}}{\partial \tilde{x}_s}$,	$\dfrac{D\tilde{u}_s^{(0)}}{Dt} - \left(\dfrac{f^2}{\omega_s^2}\right)\tilde{v}_s^{(0)} = -\dfrac{\partial \tilde{p}_s^{(0)}}{\partial \tilde{x}_s}$,	$\dfrac{\partial \tilde{u}_s^{(0)}}{\partial t} - \left(\dfrac{f^2}{\omega_s^2}\right)\tilde{v}_s^{(0)} = -\dfrac{\partial \tilde{p}_s^{(0)}}{\partial \tilde{x}}$
	$\dfrac{D\tilde{v}_s^{(0)}}{Dt} + \tilde{u}_s^{(0)} = 0$	$\dfrac{\partial \tilde{v}_s^{(0)}}{\partial t} + \tilde{u}_s^{(0)} = 0$
$\dfrac{D\tilde{w}_s^{(0)}}{Dt} = -\left(\dfrac{m_s^2}{k_s^2}\right)\left[\dfrac{\partial \tilde{p}_s^{(0)}}{\partial \tilde{z}_s} + \tilde{\rho}_s'^{(0)}\right]$	$\dfrac{D\tilde{w}_s^{(0)}}{Dt} = -\left(\dfrac{m_s^2}{k_s^2}\right)\left[\dfrac{\partial \tilde{p}_s^{(0)}}{\partial \tilde{z}_s} + \tilde{\rho}_s'^{(0)}\right]$	$\dfrac{\partial \tilde{w}_s^{(0)}}{\partial t} = -\left(\dfrac{m_s^2}{k_s^2}\right)\left[\dfrac{\partial \tilde{p}_s^{(0)}}{\partial \tilde{z}_s} + \tilde{\rho}_s'^{(0)}\right]$
$\dfrac{D\tilde{\rho}_s'^{(0)}}{Dt} = -\left(\dfrac{k_s^2}{m_s^2}\dfrac{N^2}{\omega_s^2}\right)\tilde{w}_s^{(0)}$	$\dfrac{D\tilde{\rho}_s'^{(0)}}{Dt} = -\left(\dfrac{k_s^2}{m_s^2}\dfrac{N^2}{\omega_s^2}\right)\tilde{w}_s^{(0)}$	$\dfrac{\partial \tilde{\rho}_s'^{(0)}}{\partial t} = -\left(\dfrac{k_s^2}{m_s^2}\dfrac{N^2}{\omega_s^2}\right)\tilde{w}_s^{(0)}$
$\dfrac{\partial \tilde{u}_s^{(0)}}{\partial \tilde{x}_s} + \dfrac{\partial \tilde{w}_s^{(0)}}{\partial \tilde{z}_s} = 0$	$\dfrac{\partial \tilde{u}_s^{(0)}}{\partial \tilde{x}_s} + \dfrac{\partial \tilde{w}_s^{(0)}}{\partial \tilde{z}_s} = 0$	$\dfrac{\partial \tilde{u}_s^{(0)}}{\partial \tilde{x}_s} + \dfrac{\partial \tilde{w}_s^{(0)}}{\partial \tilde{z}} = 0$
where	where	where
$\dfrac{D}{Dt} = \dfrac{\partial}{\partial \tilde{t}_s} + \tilde{u}_l^{(0)}\dfrac{\partial}{\partial \tilde{x}_s}$	$\dfrac{D}{Dt} = \dfrac{\partial}{\partial \tilde{t}} + \tilde{u}_l^{(0)}\dfrac{\partial}{\partial \tilde{x}_s} + \tilde{w}_l^{(0)}\dfrac{\partial}{\partial \tilde{z}_s}$	
$\tilde{w}_s^{(0)} = \tilde{u}_l^{(0)}\dfrac{\partial \tilde{h}}{\partial \tilde{x}_s}$ at $z = 0$	$\tilde{w}_s^{(0)} = \tilde{u}_l^{(0)}\dfrac{\partial \tilde{h}}{\partial \tilde{x}_s}$ at $z = 0$	$\tilde{w}_s^{(0)} = \tilde{u}_l^{(0)}\dfrac{\partial \tilde{h}}{\partial \tilde{x}_s} + \tilde{h}\dfrac{\partial \tilde{u}_l^{(0)}}{\partial \tilde{x}}$ at $z = 0$

$\Delta \sim 1$

$\omega_s \gg \omega_l$ (i.e., $k_s U_l/\omega_l \gg 1$)	$\omega_s \sim \omega_l$ (i.e., $k_s U_l/\omega_l \sim 1$)	$\omega_s \to \omega_l$ (i.e., $k_s U_l/\omega_l \ll 1$)
$\dfrac{D\tilde{u}_s^{(0)}}{Dt} + \tilde{w}_s^{(0)}\dfrac{\partial \tilde{u}_l^{(0)}}{\partial \tilde{z}} = -\dfrac{\partial \tilde{p}_s^{(0)}}{\partial \tilde{x}_s}$	$\dfrac{D\tilde{u}_s^{(0)}}{Dt} + A_s(\tilde{u}_l^{(0)}) - \left(\dfrac{f^2}{\omega_s^2}\right)\tilde{v}_s^{(0)} = -\dfrac{\partial \tilde{p}_s^{(0)}}{\partial \tilde{x}}$	
	$\dfrac{D\tilde{v}_s^{(0)}}{Dt} + A_s(\tilde{v}_l^{(0)}) + \tilde{u}_s^{(0)} = 0$	
$\dfrac{D\tilde{w}_s^{(0)}}{Dt} = -\left(\dfrac{m_s^2}{k_s^2}\right)\left[\dfrac{\partial \tilde{p}_s^{(0)}}{\partial \tilde{z}} + \tilde{\rho}_s'^{(0)}\right]$	$\dfrac{D\tilde{w}_s^{(0)}}{Dt} + A_s(\tilde{w}_l^{(0)}) = -\left(\dfrac{m_s^2}{k_s^2}\right)\left[\dfrac{\partial \tilde{p}_s^{(0)}}{\partial \tilde{z}} + \tilde{\rho}_s'^{(0)}\right]$	No scattered waves
$\dfrac{D\tilde{\rho}_s'^{(0)}}{Dt} + \tilde{w}_s^{(0)}\dfrac{\partial \tilde{\rho}_l'^{(0)}}{\partial \tilde{z}} = -\left(\dfrac{k_s^2}{m_s^2}\dfrac{N^2}{\omega_s^2}\right)\tilde{w}_s^{(0)}$	$\dfrac{D\tilde{\rho}_s'^{(0)}}{Dt} + A_s(\tilde{\rho}_l'^{(0)}) = -\left(\dfrac{k_s^2}{m_s^2}\dfrac{N^2}{\omega_s^2}\right)\tilde{w}_s^{(0)}$	(Reflection)
$\dfrac{\partial \tilde{u}_s^{(0)}}{\partial \tilde{x}_s} + \dfrac{\partial \tilde{w}_s^{(0)}}{\partial \tilde{z}} = 0$	$\dfrac{\partial \tilde{u}_s^{(0)}}{\partial \tilde{x}} + \dfrac{\partial \tilde{w}_s^{(0)}}{\partial \tilde{z}} = 0$	
where	where $A_s(\phi) = \tilde{u}_s^{(0)}\dfrac{\partial \phi}{\partial \tilde{x}} + \tilde{w}_s^{(0)}\dfrac{\partial \phi}{\partial \tilde{z}}$	
$\dfrac{D}{Dt} = \dfrac{\partial}{\partial \tilde{t}_s} + \tilde{u}_l^{(0)}\dfrac{\partial}{\partial \tilde{x}_s}$	$\dfrac{D}{Dt} = \dfrac{\partial}{\partial \tilde{t}} + \tilde{u}_l^{(0)}\dfrac{\partial}{\partial \tilde{x}} + \tilde{w}_l^{(0)}\dfrac{\partial}{\partial \tilde{z}}$	
$\tilde{w}_s^{(0)} = \tilde{u}_l^{(0)}\dfrac{\partial \tilde{h}}{\partial \tilde{x}_s}$ at $z = 0$	$\tilde{w}_s^{(0)} = \tilde{u}_l^{(0)}\dfrac{\partial \tilde{h}}{\partial \tilde{x}} + \tilde{h}\dfrac{\partial \tilde{u}_l^{(0)}}{\partial \tilde{x}}$ at $z = 0$	

δ_ω, δ_k, or δ_m is $O(1)$, quit applying the multiple scale method along the corresponding direction (e.g., if $\delta_\omega \sim 1$, then substitute $\delta_\omega = 1$ and set $\partial/\partial \tilde{t}_s + \delta_\omega \partial/\partial \tilde{t}_l$ back to $\omega_s \partial/\partial \tilde{t}$); (iii) relate ϵ and δ in a manner similar to relating δ and Δ by assuming that $\epsilon^m \sim \delta$; (iv) expand the variables with respect to δ in a manner similar to (5.33); and (v) substitute the above parameters and variables into the nondimensional equations and boundary condition (5.22) and (5.29)–(5.32) and rearrange them with respect to δ, noting that $k_s U_l/\omega_s \sim 1$ when $\delta_\omega \lesssim 1$ while $k_s U_l/\omega_s \sim \delta_\omega$ when $\delta_\omega \gg 1$. Then we obtain equations of various orders for various regimes.

The leading-order equations in both δ and ϵ for the various regimes are shown in Table 2. The equations and/or the bottom boundary condition are different for different parameter regimes. The difference in the

governing equations implies that the dispersion relation of scattered waves differs and hence affects the determination of the vertical wavenumber of scattered waves, the propagation after the scattering, and so on.

The governing equations and the bottom boundary condition used in section 2 correspond to those in the regime where $\omega_s \sim \omega_l$ and $\Delta \ll 1$ (and hence $k_s U_l/\omega_l \sim 1$ and $k_i/k_s \ll 1$). Note that the equations of this regime include the leading-order equations of the other two regimes ($k_s U_l/\omega_l \gg 1$ and $\ll 1$) in the corresponding limits when $\delta^n \sim \Delta \ll 1$, where $n \geq 1$ for $k_s U_l/\omega_l \gg 1$. Accordingly, the examination of the intermediate regime $k_s U_l/\omega_l \sim 1$ will reveal the basic concept of scattered waves in these three regimes. In contrast, the neglect of the advection of the primary wave field assumed in section 2 is no longer appropriate for highly nonlinear waves for which $\Delta \sim 1$. Other features of the governing equations and the bottom boundary condition are described as follows:

When $\omega_s \sim \omega_l$ and $\Delta \ll 1$ (and hence $k_s U_l/\omega_l \sim 1$ and $k_i/k_s \ll 1$): The equations in this intermediate regime $\omega_s \sim \omega_l$ for an approximately linear incident wave ($\Delta \ll 1$) to the zeroth order in both δ and ϵ are those shown in section 2. The equations are quasi-linear and thus have nearly sinusoidal solutions.

When $\omega_s \gg \omega_l$ and $\Delta \ll 1$ (i.e., $k_s U_l/\omega_l \gg 1$ and $k_i/k_s \ll 1$): The leading-order equations in this regime are almost the same as those when $\omega_s \sim \omega_l$ and $\Delta \ll 1$, if we consider the case that $\delta \sim \Delta$. (The order of ϵ is not very important as long as $\epsilon^m \sim \delta \ll 1$). The differences are twofold. First, $\tilde{v}_s^{(0)} = 0$ because f^2/ω_s^2 is smaller than δ_ω ($= \delta$). Second, the vertical advection term disappears in the leading order; that is,

$$\frac{D}{Dt} = \frac{\partial}{\partial \tilde{t}_s} + \tilde{u}_l^{(0)} \frac{\partial}{\partial \tilde{x}_s}. \tag{5.35}$$

When $\omega_s \ll \omega_l$ and $\Delta \ll 1$ (and hence $k_s U_l/\omega_l \sim 1$ and $k_i/k_s \ll 1$): The small-scale equations in this regime are complicated. Because $\omega_s \ll \omega_l$, the incident and primary reflected waves have a small time scale whereas the scattered wave field has a large time scale. Further, the leading-order equations become

$$\tilde{w}_l^{(0)} \frac{\partial \phi_s^{(0)}}{\partial \tilde{z}_s} = 0 \tag{5.36}$$

when $f \sim \omega_s$, where $\phi_s^{(0)}$ is the scattered wave variable of the zeroth order, and the equations for the next-order scattered waves involve the higher-order terms. The derivation of appropriate equations needs a careful treatment and is omitted here.

When $\omega_s \to \omega_l$ and $\Delta \ll 1$ (i.e., $k_s U_l/\omega_l \ll 1$ and $k_i/k_s \sim 1$): This is the regime that previous studies have considered. Indeed, we regain the usual linear scattered-wave equations from the nondimensionalized Eqs. (5.22) and (5.29)–(5.32), noting that $k_s U_l/\omega_s \sim \Delta\delta_\omega\delta_k^{-1} \sim \Delta$.

When $\Delta \sim 1$: Even for a highly nonlinear incident wave ($\Delta \sim 1$), the governing equations are tractable in the regime $\omega_s \gg \omega_l$. The equations of the leading order (δ^0) are the same as those for $\Delta \ll 1$ and $\omega_s \gg \omega_l$, except for two differences. One difference is that the multiple scale method is not applicable to the z direction. The other is that both the momentum equation for the x direction and the density equation now include the advection of the large-scale variables by the scattered wave (i.e., $\tilde{w}_s^{(0)}\partial\tilde{u}_l^{(0)}/\partial\tilde{z}$ and $\tilde{w}_s^{(0)}\partial\tilde{\rho}_l'^{(0)}/\partial\tilde{z}$, respectively) at the leading order.

As for the other two regimes, the leading-order equations become nonlinear in the regime $k_s U_l/\omega_l \sim 1$ (and $\omega_s \sim \omega_l$) and scattering hardly occurs in the regime $k_s U_l/\omega_l \ll 1$ (i.e., $\omega_s \to \omega_l$).

6. Effects and implications

Some possible effects and implications of frequency change on scattering are discussed in this section. The discussion, however, is limited to showing that these are likely to occur and leaves quantitative investigations for future works.

a. Effects on the change in vertical wavenumber

The change in the vertical wavenumber upon scattering is considered to be important for causing boundary mixing. Thus, the effects of frequency change on the change in the vertical wavenumber upon scattering are discussed first.

Consider the ratio of the vertical wavenumber of scattered waves (m_s) to that estimated assuming frequency conservation (m_{s0}). It is given by

$$\left|\frac{m_s}{m_{s0}}\right| = \left(\frac{N^2 - \omega_s^2}{N^2 - \omega_i^2}\right)^{1/2} \left(\frac{\omega_i^2 - f^2}{\omega_s^2 - f^2}\right)^{1/2}, \tag{6.1}$$

since the vertical wavenumber is determined from the dispersion relation (2.8) and the horizontal wavenumbers are the same. To consider the basic change according to the parameter regimes, let us approximate the dispersion relation as $\omega \simeq Nk/m$. Then, the above ratio becomes

$$\left|\frac{m_s}{m_{s0}}\right| \simeq \left|\frac{\omega_i}{\omega_s}\right| \approx \left|\frac{k_s u_l}{\omega_i} \pm 1\right|^{-1}, \tag{6.2}$$

where $u_l = u_i + u_r$ [given in (2.21)]. This states that the change in the vertical wavenumber depends on the

TABLE 3. Change in vertical wavenumber due to frequency change when $\Delta \ll 1$; $m_{s\pm}$ and m_{s0} are the vertical wavenumbers of the scattered waves and those calculated by assuming frequency conservation, respectively. Subscripts s and i represent the scattered and incident waves, respectively, and subscripts + and − denote the sum and difference frequency waves, respectively.

Regime	$k_s U_{i+r}/\omega_l \gg 1$	$k_s U_{i+r}/\omega_l \sim 1$		
Intrinsic frequency	$\omega_s \gg \omega_i$	$\omega_s \sim \omega_i$		$\omega_s \ll \omega_i$
Vertical wavenumber	$m_{s\pm} \ll m_{s0}$	$m_{s+} < m_{s0}$	$m_{s-} > m_{s0}$	$m_{s-} \gg m_{s0}$

nondimensional parameter $k_s U_{i+r}/\omega_i$, which is a measure of frequency change (4.1) because $U_{i+r} = U_l = 2U_i$ in section 2. This dependence is summarized in Table 3.

When $k_s U_{i+r}/\omega_i \gg 1$ (i.e., the lee-wave regime), the vertical wavenumber of the scattered waves is much lower than that estimated assuming frequency conservation. This is less favorable for causing boundary mixing. When $k_s U_{i+r}/\omega_i \sim 1$ (i.e., the MTL wave regime) and $\omega_s \sim \omega_i$, the values of m_s and m_{s0} are different but are on the same order. The vertical wavenumber of the sum waves ($|k_s u_l/\omega_i| + 1$) becomes lower (i.e., $m_s < m_{s0}$), whereas that of the difference waves ($|k_s u_l/\omega_i| - 1$) becomes higher. The former is less favorable for boundary mixing; the latter is more favorable. In particular, when $\omega_s \ll \omega_i$, the vertical wavenumber becomes much higher (i.e., $m_s \gg m_{s0}$), which is favorable for boundary mixing.

In this manner, the occurrence of frequency change affects the energy redistribution in the vertical wavenumber space. Accordingly, the estimates of boundary mixing due to internal wave scattering based on the energy redistribution in the vertical wavenumber can be affected by the frequency change.

b. Horizontal phase velocity

The horizontal phase velocity of the scattered waves relative to the moving fluid becomes [from (3.2)]

$$c_{\mathrm{rp}} = \frac{\omega}{\theta_b k_b} = -u_l\big|_{z=0,t=t_0} \pm \frac{\omega_i}{k_b} = 2U_i\left[-\frac{u_l\big|_{z=0,t=t_0}}{2U_i} \pm \left(\frac{2k_b U_i}{\omega_i}\right)^{-1}\right]. \tag{6.3}$$

The ratio $2k_b U_i/\omega_i$, which corresponds to (4.1), characterizes the scattered-wave propagation. Because the magnitude of the nondimensional advecting flow, $|u_l/2U_i|$, does not exceed unity, the propagation of scattered waves is dominated or deeply affected by the advection due to the primary wave field when $2k_b U_i/\omega_i \gg 1$ (the lee-wave regime) or when $2k_b U_i/\omega_i \sim 1$ (the MTL wave regime), respectively. In contrast, when the frequency change is negligible (i.e., $2k_b U_i/\omega_i \ll 1$), the advection is not effective.

When viewed in the frame fixed to the ground, the horizontal phase velocity nearly vanishes (i.e., $c_{\mathrm{rp}} + u_l|_{z=0} \approx 0$) at the time of the generation in the lee-wave regime. Accordingly, the scattered waves are trapped horizontally at the generation site and could effectively grow through superposition. The scattered-wave propagation has many similarities to that of the tidally generated internal waves presented in Nakamura and Awaji (2001).

c. Critical levels

As well as the advection of scattered waves, the flow associated with the primary wave field will cause the refraction of scattered waves as the waves propagate away from the generation site. One interesting implication of this is the presence of critical levels, where $U - c_p = \pm f/k$ and where the wave energy converges and can cause mixing and background-flow acceleration (cf. LeBlond and Mysak 1978). In the present case, c_p is the horizontal phase velocity of the scattered waves observed in the frame fixed to the ground and is given as

$$c_p = \pm \frac{\omega_i}{k_b} \tag{6.4}$$

at the time of the generation. The background horizontal flow velocity U is associated with the large-scale waves u_l and thus its maximum absolute value becomes $2U_i$. Using these values, a critical level can be present if

$$2U_i - \omega_i/k_b \geq -f/k_b. \tag{6.5}$$

At the same time, the condition for frequency change states from (4.1) that the primary wave field has the maximum flow speed of $2U_i \gtrsim \omega_i/k_b$. Hence, in most cases, there are one or more critical levels within one vertical wavelength of the large-scale waves ($2\pi/m_i$). In such cases, a large portion of the scattered waves could encounter a critical level somewhere in the course of their upward propagation.

In particular, scattered waves would encounter a critical level when they propagate upward so fast that with the initial group velocity, the waves would travel over the distance $2\pi/m_i$ before the temporal variation of the large-scale wave field can become significant; that is,

$$\left|\frac{(2\pi/\omega_i)}{(2\pi/m_i)/c_{gz}}\right| \gg 1. \tag{6.6}$$

Here, c_{gz} is the initial vertical group velocity of the scattered waves and can be approximated as $-\omega_s/m_s$ when $N^2 \gg \omega_s^2 \gg f^2$. Using the scattered wave frequency (3.2), (6.6) becomes

$$\frac{(2\pi/\omega_i)}{(2\pi/m_i)/c_{gz}} \approx \frac{m_i}{\omega_i}\frac{1}{Nk_s}(k_s u_l \pm \omega_i)^2 \approx \frac{k_i}{k_s}\left(\frac{k_s u_l}{\omega_i} \pm 1\right)^2 \gg 1, \tag{6.7}$$

where the condition $N^2 \gg \omega_i^2 \gg f^2$ is also used and where $k_s \approx k_b$, in the present parameter range. The above situation can take place in the lee-wave regime where $k_s u_l/\omega_i \gg 1$, if k_b is sufficiently high that

$$\Delta^2 \gg \delta_k \tag{6.8}$$

is satisfied. In this situation, the scattered waves will encounter a critical level within one vertical incident wavelength from the bottom and a large portion of the waves will be absorbed there, causing both mixing and the acceleration of the large-scale wave flow.

This suggests the possibility that the scattered waves of the lee-wave regime could break at a level well above the bottom when generated by an incident wave of a low vertical mode or could break near the bottom when generated by an incident wave of a high vertical mode.

d. Nonmonochromatic incident waves

Thus far, we have focused on the case in which the incident wave was monochromatic. In realistic situations, however, incident waves are usually polychromatic and the flow often has a steady component. A solution for nonmonochromatic incident waves can be obtained in a similar fashion to section 2, as long as $\Delta \ll 1$ so that the incident waves can be linearly superposed. (A solution for the topography considered above can be easily obtained but is omitted for conciseness.)

In such a case, the Doppler shift ($-k_b u_l$) is caused by the total large-scale flow associated with all of the incident waves, their primary reflected waves, and other flow components. However, if a scattered-wave solution is obtained separately for each incident-wave Fourier component, the Doppler shift term does not take the total flow into account, but only the flow associated with only one incident-wave component and its primary reflected wave. Because of this difference in the Doppler shift, the scattered wave frequency and hence the vertical wavenumber are not correctly obtained from a solution for each incident-wave component.

The above argument has an important implication that, in the parameter regimes where the frequency change occurs, the scattered waves associated with nonmonochromatic incident waves can no longer be represented by the superposition of the scattered wave solutions obtained separately for each incident-wave Fourier component. This fact will make it difficult to analytically estimate the energy made available for mixing due to scattering.

7. Summary

The scattering of internal gravity waves off a rough topography redistributes the incoming energy flux in the wavenumber space, which often causes enhanced cross-isopycnal mixing near the bottom (boundary mixing). This process is considered to contribute significantly to the globally averaged mixing and could affect the global thermohaline circulation (e.g., Müller and Xu 1992). In previous studies on such internal wave scattering and/or reflection, it was assumed that the frequency is conserved. However, the present study has shown that the frequency changes during reflection from a rough topography in a certain parameter range, which includes the realistic range.

To demonstrate this fact analytically, we have derived sets of appropriate and tractable governing equations for scattered waves by a scaling argument, assuming that the amplitude of the topography is small. The derivation procedure has two points: the use of the multiple scale method and the definition of a scattered wave field.

The multiple scale method is useful because in most cases, the scattered waves and the incident (and primary reflected) waves have very different scales in time and/or space when change in frequency occurs, as argued in section 4. The ratios of the scales of the scattered and incident waves, in turn, can be determined using the dispersion relation and the condition for the change in the frequency; they are summarized in Table 1.

Also, for a clear separation of the scattered waves and incident and primary reflected waves, we define the scattered wave field as the difference between the total wave field and the wave field created by the reflection on a plane. This definition roughly corresponds to the expansion of the wave field with the nondimensional topographic height scale ϵ. The definition requires that the incident and primary reflected wave field exactly satisfy the governing equations, and thus it simplifies the treatment of incident waves even in the nonlinear regime.

The combination of these two points allows us to systematically derive the leading-order equations for various parameter regimes; that is, $\Delta \ll$ or ~ 1, and/or $K_b U_{i+r}/\omega_i \ll$, $\sim$, or $\gg 1$, where Δ is the wave Froude

number for the incident waves and K_b, U_{i+r}, and ω_i are the topographic wavenumber (which is on the order of the scattered wave wavenumber), the flow amplitude of the sum of incident and primary reflected waves, and the incident-wave frequency, respectively. Although a heuristic argument such as the one described in section 2 is helpful for understanding the basic idea, the lengthy but more rigorous derivation shown in section 5, which provides the order of each term, is useful for the further development of the theory. For example, the method shown here also enables us to derive higher-order equations (although the equations are not shown for conciseness). In addition, the extension to a three-dimensional case or to the case with a mean slope is straightforward although the equations shown here are for a vertically two-dimensional case with no mean slope.

A solution in the parameter regime $\delta_\omega \sim 1$ and $\Delta \ll 1$ (i.e., $K_b U_{i+r}/\omega_i \sim 1$ and $K_i/K_b \ll 1$, where K_i is the horizontal wavenumber of an incident wave) is shown for a simple case in which both the incident wave and the topographic roughness are monochromatic. This solution is archetypal because it includes those in the other two regimes of $K_b U_{i+r}/\omega_i \gg$ and $\ll 1$ in the corresponding limits, when $\Delta \ll 1$.

The solution indicates that the intrinsic frequencies of the scattered waves are the sum and difference of the incident-wave frequency and the Doppler shift (or the frequency of quasi-steady lee waves). This Doppler shift causes the change in the frequency. Hence, the assumption of frequency conservation is not valid if the Doppler shift is significant. This condition is met in the case that the horizontal scale of the bottom roughness (or the length scale on the plane of the slope) is on the order of, or much smaller than, that of the incident-wave flow excursion, since the horizontal wavenumber of the scattered waves is mainly determined from that of the bottom roughness in this parameter regime. Simple estimates of this condition in section 4a suggest that the frequency change could be a common phenomenon in the ocean.

The underlying physics of the frequency change is the same as that in the case of the internal wave generation by a barotropic tidal flow over a topographic feature, which was shown in earlier investigations by Nakamura et al. (2000) and Nakamura and Awaji (2001); nevertheless, the generalization to internal wave scattering has various implications, such as those summarized below.

First, the frequency change in the scattering affects the energy redistribution in the vertical wavenumber space. This will in turn influence the strength of the internal wave-induced boundary mixing. In addition, the resulting energy redistribution in the frequency space could affect the shape of the internal wave spectra, at least locally. Second, when the frequency change occurs, the scattered waves are affected significantly by the background flow associated with the incident and primary reflected waves. This results in the advection of the scattered waves so that the waves are arrested horizontally near the generation site and superposed to grow. Further, the background flow causes the refraction of the scattered waves. In most cases, critical levels appear and can cause both mixing and flow acceleration. In particular, the scattered waves in the lee-wave regime (i.e., $K_b U_{i+r}/\omega_i \gg 1$) would encounter a critical level, which can take place well above the bottom for low-vertical-mode incident waves and near the bottom for high-mode incident waves. Finally, the scattered waves associated with nonmonochromatic incident waves cannot be obtained by summing the solutions for each incident-wave Fourier component even at the leading order if the frequency changes. This is because the Doppler shift depends on the total flow at the bottom.

These results suggest that an estimate of the energy redistribution under the frequency change would be one of the necessary steps toward estimating the boundary mixing induced by the scattering and in understanding the maintenance of the spectrum shape of oceanic internal waves, which affects both interior and boundary mixing. For this goal, important issues still remain. For example, the effects of large-amplitude topography, wave nonlinearity, polychromatic incident waves, and nonconstant N are out of scope of this study. In particular, the consideration of large-amplitude topography is important because the ratio of the amplitude of the scattered and incident waves is on the order of the nondimensional topographic-height scale $\epsilon = Hm_s$ and hence is much less than unity for a small-amplitude topography, as the scaling argument in section 5b(2) suggested. These effects should be included for the application to the realistic situation and are left for future works.

Acknowledgments. We sincerely appreciate the helpful comments of three anonymous reviewers. This study was supported by Category 7 of the MEXT RR2002 Project for Sustainable Coexistence of Humans, Nature and the Earth and by a Grant-in-Aid for the 21st Century COE Program (Kyoto University, G3). T.N. was partly supported by Grant-in-Aid for Scientific Research. This study was done when T.N. was with the Department of Geophysics, Kyoto University.

APPENDIX A

Applicability around $\omega \sim N$ or $\omega \sim f$

For scaling the ratios δ_ω , δ_k, and δ_m in section 5a(4), we used the approximate dispersion relation ($\omega \simeq Nk/m$)

that results in relation (5.9), $\delta_\omega \sim \delta_k/\delta_m$. This approximation of the dispersion relation becomes invalid as ω approaches N or f. Here, we consider the frequency range in which δ_ω is on the order of δ_k/δ_m so that relation (5.9) is valid, and thus the scalings in section 5 based on this relation are appropriate.

When $\omega \sim N$, the dispersion relation (2.13) can be usually approximated as

$$\omega^2 = \frac{N^2k^2}{k^2 + m^2} \tag{A.1}$$

because $N \gg f$ in most cases. Hence, if $k^2 + m^2$ and m^2 are on the same order, ω is on the order of Nk/m and hence (5.9) is valid. This condition is met if $k^2 \lesssim m^2$, that is,

$$\omega^2 \lesssim \frac{N^2}{2}. \tag{A.2}$$

Similarly, when $\omega \sim f$, the hydrostatic approximation is usually valid, so that

$$\omega^2 = \frac{N^2k^2}{m^2} + f^2. \tag{A.3}$$

Accordingly, (5.9) is valid when $N^2k^2/m^2 \gtrsim f^2$. This condition can be rewritten using (A.3) as

$$\omega^2 \gtrsim \frac{f^2}{2}. \tag{A.4}$$

This condition may be relaxed to some extent, if both the incident frequency and the scattered frequency are on the order of f (i.e., $\omega_l \sim \omega_s \sim f$). The ratio δ_k/δ_m now becomes

$$\frac{\delta_k^2}{\delta_m^2} = \frac{\omega_l^2 - f^2}{\omega_s^2 - f^2}. \tag{A.5}$$

Thus, when the inequalities

$$\frac{1}{10}\delta_\omega^2 < \frac{\omega_l^2 - f^2}{\omega_s^2 - f^2} < 10\delta_\omega^2 \tag{A.6}$$

are satisfied, δ_ω and δ_k/δ_m are on the same order. The inequalities can be approximated as

$$\omega_l > \frac{\sqrt{10}}{3}f \quad \text{and} \quad \omega_s > \frac{\sqrt{10}}{3}f, \tag{A.7}$$

assuming $\omega_s \sim \omega_l$, which yields $10\omega_s \gg \omega_l$ and $10\omega_l \gg \omega_s$. Because $\sqrt{10}/3 \simeq 1.054$, the intrinsic frequency should be greater than f by at least 5% for the scaling in section 5 to be applicable.

APPENDIX B

Nondimensional Topographic Height Scale ϵ

The nondimensional scale of topographic height (ϵ) used in section 5 is defined here based on the assumption of a small-amplitude topography, which consists of two conditions: (i) The height of the topography is much smaller than the vertical scale of the waves under consideration and (ii) the slope of the topography is smaller than the wave ray slope.

Condition (i) is required to expand the bottom boundary condition at $z = 0$ and is satisfied if

$$Hm_l \ll 1 \quad \text{and} \quad Hm_s \ll 1, \tag{B.1}$$

where H is the topographic height scale introduced in section 5a(3). These two inequalities are satisfied if

$$\epsilon_1 = Hm_s \ll 1, \tag{B.2}$$

because $\delta_m (= m_l/m_s)$ is much smaller than or on the order of unity, as shown in Table 1.

Condition (ii) states that there is no critical or supercritical slope. This condition is met if

$$k_bH\frac{m_l}{k_l} < 1 \quad \text{and} \quad k_bH\frac{m_s}{k_s} < 1, \tag{B.3}$$

where k_b is the wavenumber of the corresponding topographic Fourier component. When $\omega_s \gg \omega_l$ or $\omega_s \sim \omega_l$, these inequalities are satisfied if

$$\epsilon_2 = \frac{k_b}{k_l}Hm_l < 1, \tag{B.4}$$

since $|m_s/k_s|/|m_l/k_l| \sim \omega_l/\omega_s \lesssim 1$ in these regimes using the approximate dispersion relation, $\omega \simeq N|k/m|$. Conversely, when $\omega_s \ll \omega_l$, (B.3) requires

$$\epsilon_2 = \frac{k_b}{k_s}Hm_s \sim Hm_s < 1, \tag{B.5}$$

where the scaling $k_b \sim k_s$ is used (see section 4b).

The scales ϵ_1 and ϵ_2 are related as follows:

$$\begin{aligned} \epsilon_1 &\sim \frac{\delta_k}{\delta_m}\epsilon_2 \quad \text{for } \omega_s \gg \omega_l, \\ &\sim \frac{\delta_k}{\delta_m}\epsilon_2 \sim \epsilon_2 \quad \text{for } \omega_s \sim \omega_l, \\ &\sim \epsilon_2 \quad \text{for } \omega_s \ll \omega_l. \end{aligned} \tag{B.6}$$

Either ϵ_1 or ϵ_2 is available for the expansion of the bottom boundary condition and/or the reflected wave field. Here, we choose ϵ_1 as the nondimensional topographic height scale ϵ because the definition of ϵ_2 is not common to the three-parameter regimes. From (B.6) and (B.5), conditions (i) and (ii) can be written in terms of ϵ as

$$\epsilon(=\epsilon_1) \lesssim \frac{\delta_k}{\delta_m}(\sim\delta) \ll 1 \quad \text{for } \omega_s \gg \omega_l,$$
$$\ll 1 \quad \text{for } \omega_s \sim \omega_l \quad \text{or } \omega_s \ll \omega_l. \qquad \text{(B.7)}$$

Note that the relation between ϵ and δ is specified by the above scaling only in the case

$$\omega_s \gg \omega_l.$$

REFERENCES

Baines, P. G., 1971a: The reflexion of internal/inertial waves from bumpy surfaces. *J. Fluid Mech.,* **46,** 273–291.

——, 1971b: The reflexion of internal/inertial waves from bumpy surfaces. Part 2. Split reflexion and diffraction. *J. Fluid Mech.,* **49,** 113–131.

——, 1995: *Topographic Effects in Stratified Flow*. Cambridge University Press, 498 pp.

Balmforth, N. J., G. R. Ierley, and W. R. Young, 2002: Tidal conversion by subcritical topography. *J. Phys. Oceanogr.,* **32,** 2900–2914.

Bell, T. H., 1975a: Lee waves in stratified flows with simple harmonic time dependence. *J. Fluid Mech.,* **67,** 705–722.

——, 1975b: Topographically generated internal waves in the open ocean. *J. Geophys. Res.,* **80,** 320–327.

Bryan, F., 1987: Parameter sensitivity of primitive equation ocean general circulation models. *J. Phys. Oceanogr.,* **17,** 970–985.

Eriksen, C. C., 1982: Observation of internal wave reflection from sloping bottoms. *J. Geophys. Res.,* **87,** 525–538.

——, 1985: Implications of ocean bottom reflection for internal wave spectra and mixing. *J. Phys. Oceanogr.,* **15,** 1145–1156.

Gilbert, D., and C. Garrett, 1989: Implications for ocean mixing of internal wave scattering off irregular topography. *J. Phys. Oceanogr.,* **19,** 1716–1729.

Hasumi, H., and N. Suginohara, 1999: Effects of locally enhanced vertical diffusivity over rough bathymetry on the world ocean circulation. *J. Geophys. Res.,* **104,** 23 367–23 374.

Johnston, T. M. S., and M. A. Merrifield, 2003: Internal tide scattering at seamounts, ridges, and islands. *J. Geophys. Res.,* **108,** 3180, doi:10.1029/2002JC001528.

Khatiwala, S., 2003: Generation of internal tides in an ocean of finite depth: Analytical and numerical calculations. *Deep-Sea Res.,* **50,** 3–21.

Lamb, K. G., 2004: Nonlinear interaction among internal wave beams generated by tidal flow over supercritical topography. *Geophys. Res. Lett.,* **31,** L09313, doi:10.1029/2003GL019393.

LeBlond, P. H., and L. A. Mysak, 1978: *Waves in the Ocean*. Elsevier Scientific, 602 pp.

Legg, S., 2004: Internal tides generated on a corrugated continental slope. Part I: Cross-slope barotropic forcing. *J. Phys. Oceanogr.,* **34,** 156–173.

——, and A. Adcroft, 2003: Internal wave breaking at concave and convex continental slopes. *J. Phys. Oceanogr.,* **33,** 2224–2246.

Lighthill, M. J., 1978: *Waves in Fluids*. Cambridge University Press, 504 pp.

Mied, R. P., and J. P. Dugan, 1976: Internal wave reflexion from a sinusoidally corrugated surface. *J. Fluid Mech.,* **76,** 259–272.

Müller, P., and N. Xu, 1992: Scattering of oceanic internal gravity waves off random bottom topography. *J. Phys. Oceanogr.,* **22,** 474–488.

——, and X. Liu, 2000a: Scattering of internal waves at finite topography in two dimensions. Part I: Theory and case studies. *J. Phys. Oceanogr.,* **30,** 532–549.

——, and ——, 2000b: Scattering of internal waves at finite topography in two dimensions. Part II: Spectral calculations and boundary mixing. *J. Phys. Oceanogr.,* **30,** 550–563.

Munk, W. H., 1966: Abyssal recipes. *Deep-Sea Res.,* **13,** 707–730.

——, and C. Wunsch, 1998: Abyssal recipes. II: Energetics of tidal and wind mixing. *Deep Sea Res. I,* **45,** 1977–2010.

Nakamura, T., and T. Awaji, 2001: A growth mechanism for topographic internal waves generated by an oscillatory flow. *J. Phys. Oceanogr.,* **31,** 2511–2524.

——, ——, T. Hatayama, K. Akitomo, T. Takizawa, T. Kono, Y. Kawasaki, and M. Fukasawa, 2000: The generation of large-amplitude unsteady lee waves by subinertial K_1 tidal flow: A possible vertical mixing mechanism in the Kuril Straits. *J. Phys. Oceanogr.,* **30,** 1601–1621.

Phillips, O. M., 1977: *The Dynamics of the Upper Ocean*. Cambridge University Press, 336 pp.

Rubenstein, D., 1988: Scattering of inertial waves by rough bathymetry. *J. Phys. Oceanogr.,* **18,** 5–18.

St. Laurent, L., and C. Garrett, 2002: The role of internal tides in mixing the deep ocean. *J. Phys. Oceanogr.,* **32,** 2882–2899.

Thorpe, S. A., 1997: On the interactions of internal waves reflecting from slopes. *J. Phys. Oceanogr.,* **27,** 2072–2078.

——, 2001: Internal wave reflection and scatter from sloping rough topography. *J. Phys. Oceanogr.,* **31,** 537–553.